TECHNISCHE UNIVERSITÄT WIEN

DIPLOMA THESIS

Quantitative analysis of halogens in polymer coatings using Laser Induced Breakdown Spectroscopy

carried out for the purpose of obtaining the degree of

Diplom-Ingenieur (Dipl.-Ing.)

at the Institute of Chemical Technologies and Analytics, Vienna University of Technology

under the supervision of

Univ.-Prof. Dipl.-Ing. Dr.techn. **Andreas Limbeck**

and Projektass. Dipl.-Ing. **David Ken Gibbs**, BSc

by

Patrick Tapler, BSc

Vienna, 09.09.2024

_____

(Patrick Tapler)

Abstract

In today's semiconductor industry, halogenated polymer coatings are utilized as corrosion protection in microelectronic devices. In order to monitor the degradation of these anti-corrosion coatings, a spatially resolved analysis of their halogen content is required. Because methods such as Laser Ablation Inductively Coupled Plasma Mass Spectrometry (LA-ICP-MS) or X-Ray Fluorescence Spectroscopy (XRF), which would normally be used for this task, struggle with the detection of halogens, there is need for the development of a fast and quantitative imaging technique, that is able to perform measurements in the µg/g range. The method investigated in this work was Laser Induced Breakdown Spectroscopy (LIBS).

The goal of this thesis was to develop a LIBS measurement methodology that enables the quantitative analysis of F, Cl, and Br in polymer coatings. Given the low excitation efficiency of halogens, it was necessary to enhance the signals, for which there are numerous potential approaches. The two options employed in this work, however, were the application of reduced pressure, which changed the plasma dynamics resulting in an enhancement of emission line intensity, and sampling the plasma radiation directly next to the plasma plume with a fiber optic cable, referred to as 'direct sampling', which increased the collection efficiency. These could be investigated through the successful development of the 'direct stage', a custom-built ablation chamber mounted on a 3D printed stage built in-house. To be able to perform a quantitative analysis, standards were prepared by dissolving Polyimide and halogen-containing benzoic acid derivates in N-Methyl-2-pyrrolidone. After optimizing all measurement parameters, calibrations were performed, and the raw data was normalized using different normalization methods.

A pressure of 50 mbar significantly improved the signal-to-background ratio (SBR) of the F I 685,6 nm emission line by a factor of ~2, resulting in a background normalized F calibration with a R^2 of 0,9988 and a LOD of 48 µg/g. The quantitative analysis of F can therefore be considered a success. Although the Cl measurements at 50 mbar exhibited higher sensitivity, the calibration under atmospheric pressure achieved better figures of merit. The background normalized Cl calibration at 1013 mbar obtained a R^2 of 0,9925 with a LOD of 1497 µg/g. Unfortunately, the use of vacuum did not have a beneficial effect on the Br I 827,3 nm emission line intensity. Therefore, the Br calibration was carried out under atmospheric pressure leading to a R^2 of 0,8615 along with a LOD of 1703 µg/g, which was the most deficient of all investigated elements. Nevertheless, this thesis shows that LIBS can be operated in a quantitative manner in the µg/g range, and that the developed vacuum method is also applicable to fluoropolymer samples from industry, as demonstrated by the analysis of a sports bag material.

Kurzfassung

In der heutigen Halbleiterindustrie finden halogenierte Polymerbeschichtungen als Korrosionsschutz in mikroelektronischen Bauelementen Verwendung. Um die Degradation dieser Korrosionsschutzschichten zu verfolgen, ist eine räumlich aufgelöste Analyse ihres Halogengehaltes erforderlich. Da Methoden wie die Laserablation-induktiv-gekoppeltes-Plasma-Massenspektrometrie (LA-ICP-MS) oder die Röntgenfluoreszenzanalyse (RFA), welche üblicherweise für Problemstellungen dieser Art eingesetzt werden, bei der Detektion von Halogenen mit Schwierigkeiten konfrontiert sind, besteht Bedarf an der Entwicklung einer schnellen und quantitativen Imagingtechnik, die über Nachweisgrenzen im µg/g-Bereich verfügt. Die in dieser Arbeit auf ihre Anwendbarkeit untersuchte Methode war die Laserinduzierte Plasmaspektroskopie (LIBS).

Ziel dieser Arbeit war die Methodenentwicklung einer LIBS-Technik, die die quantitative Analyse von F, Cl, und Br in Polymerbeschichtungen ermöglicht. Angesichts der niedrigen Anregungseffizienz der Halogene war es erforderlich, die Signale zu verstärken, wofür es zahlreiche Möglichkeiten gibt. Die beiden in dieser Arbeit verwendeten Techniken waren das Anlegen von reduziertem Druck, was zu einer Veränderung der Plasmadynamik und einer verbesserten Emissionslinienintensität führte, und die Messung der Plasmastrahlung in direkter Nähe des Plasmas mittels optischem Glasfaserkabel, was als „direkte Messung“ bezeichnet wurde und die Sammeleffizienz erhöhte. Dies konnte durch die erfolgreiche Fertigung einer "Direktbühne" untersucht werden, einer maßgeschneiderten Ablationskammer, welche auf einer selbst entworfenen, 3D-gedruckten Bühne montiert ist. Um die Durchführung einer quantitativen Analyse zu ermöglichen, wurden Festkörperstandards durch Lösen von Polyimid und halogenhaltigen Benzoesäurederivaten in N-Methyl-2-pyrrolidon hergestellt. Nach abgeschlossener Optimierung aller Messparameter konnten Kalibrationen gemessen werden, wobei verschiedenste Normalisierungsmethoden getestet wurden.

Ein Druck von 50 mbar führte zu einer signifikanten Verbesserung des Signal-Untergrund-Verhältnisses (SBR) der F I 685,6 nm Emissionslinie um einen Faktor von ~2, wodurch eine untergrundnormalisierte F-Kalibration mit einem R^2 von 0,9988 und einem LOD von 48 µg/g erreicht werden konnte. Die quantitative Bestimmung von F kann daher als Erfolg bewertet werden. Obwohl die Cl-Messungen bei 50 mbar eine höhere Empfindlichkeit aufwiesen, erzielte die Kalibration unter Atmosphärendruck bessere analytische Kenngrößen. Die untergrundnormierte Cl-Kalibration bei 1013 mbar wies ein R^2 von 0,9925 und einen LOD von 1497 µg/g auf. Bei der Br I 827,3 nm Emissionslinie konnte allerdings kein positiver Effekt durch die Verwendung von Vakuum beobachtet werden. Daher wurde die Br-Kalibration unter Atmosphärendruck gemessen, wodurch sich ein R^2 von 0,8615 und ein LOD von 1703 µg/g ergaben, was von allen untersuchten Elementen das schlechteste Ergebnis war. Dennoch demonstriert diese Arbeit, dass LIBS im µg/g-Bereich quantitativ betrieben werden kann, und dass die entwickelte

Vakuummethode auch auf Fluorpolymerproben aus der Industrie anwendbar ist, wie anhand der Analyse eines Sporttaschenmaterials bewiesen wird.

Danksagung

Ich möchte an dieser Stelle die Gelegenheit nützen, um allen Personen zu danken, welche mir mein Studium und im Zuge dessen auch diese Arbeit ermöglicht haben. Ein großes Danke geht an meinen Betreuer Andreas Limbeck, der mir im Labor jede freie Sekunde mit Rat und Tat zur Seite gestanden hat. Danke auch an die gesamte Forschungsgruppe für die äußerst angenehme Arbeitsatmosphäre, die fachliche Expertise, und die wahnwitzigen Diskussionen beim Mittagessen, welche so manche meiner schiefgegangenen Messungen in den Hintergrund gerückt haben. Ein besonderes Dankeschön muss ich an David Gibbs richten, ohne dessen Anleitung und Knowhow auf dem Gebiet diese Arbeit bei Weitem nicht zu solchen Ergebnissen geführt hätte.

Ein großes Dankeschön geht auch an meinen Freundeskreis, der über die Jahre hinweg mein Jammern ertragen und mich immer wieder mit vielen leckeren Bierchen vom Studium abgelenkt hat, wenn es am dringendsten nötig war.

Zu guter Letzt geht das größte Danke aber an meine Familie: Mama, Papa, Sarah, Oma, Opa. Ohne euch und eure Unterstützung, emotional wie finanziell, wäre all das nicht möglich gewesen. Ich hab‘ euch lieb und bin unendlich dankbar für alles, was ihr für mich getan habt, auch wenn ich das nicht immer so gut kommuniziere. Danke für alles.

Contents

1 Introduction

Microelectronic devices have become irreplaceable in our modern society. They are used in every electronic device but are especially important in applications like vehicles or medical equipment, where a potential failure of the device can lead to catastrophic consequences[1]. The failure of such products also has a negative impact in less critical applications, as more electronic waste is generated which is bad for the environment and depletes resources[2]. Therefore, increasing the reliability of these devices, which subsequently improves the safety and sustainability, is of paramount importance for the semiconductor industry.[3]

One major reason for the failure of electronic devices is corrosion. To prevent this, polymer coatings are used as corrosion protection. Polymers in general exhibit outstanding material properties such as chemical and weathering resistance and mechanical stability. They are also very customizable and can be adapted to various requirements which is why they are used in a wide variety of applications like membranes in proton exchange membrane fuel cells[4], sensors[5], intelligent fertilizers in agriculture[6], drug delivery systems in clinical medicine[7] or packaging materials.

Especially Polytetrafluoroethylene (PTFE), which is perhaps better known by its brand name Teflon™, possesses excellent properties making it a suitable material for anti-corrosion coatings. PTFE has high mechanical strength, hydrophobicity, chemical inertness, anti-corrosive function and thermal resistance[8,9]. While most polymers are not able to withstand high temperatures, PTFE can endure temperatures of up to 300 °C enabling it to act as a robust engineering thermoplastic. This is especially important for semiconductor products used in harsh environments where they are exposed to thermal stress.[10]

Another halogenated polymer that is widely used in semiconductor industry is the chlorine-containing PVC due to its fire retardant and chemically resistant properties. Brominated polymers are typically also used as flame retardants in moulding compounds[11] with new research exploring the possibilities of utilizing them in self-healing anticorrosive coatings[12].

The only way to improve the corrosion protection is to understand why it failed in the first place and what led to its degradation. In order to monitor the degradation of these anti-corrosion coatings, it is feasible to analyze the content and spatial distribution of halogens contained in them. This is due to carbon being a ubiquitous element ever present in the air as CO_2, tubing built into experimental devices, deposits from previous experiments or other miscellaneous sources. Halogens on the other hand are only contained in the coatings and can therefore be determined without interference – at least until spectral interferences must be considered.

The fast and quantitative determination of halogens is unfortunately still very challenging. While X-Ray Fluorescence Spectroscopy (XRF) presents certain difficulties regarding quantification, the combination of combustion with subsequent Ion Chromatography (IC) is limited to the analysis of liquids, resulting in more elaborate sample preparation. The application of solids analysis, on the other hand, allows for a faster determination of halogens. One method suited for this task, but without spatial resolution, is High-Resolution Continuum Source Atomic Absorption Spectroscopy (HR-CS-AAS)[13]. Another powerful technique that is widely used in various areas is Laser Ablation Inductively Coupled Plasma Mass Spectrometry (LA-ICP-MS), which can perform imaging as well as depth profiling for very low analyte concentrations. However, all methods utilizing ICP-MS struggle to measure halogens due to their high ionization energies, which are[14]: 17,4 eV for F[15], 13,0 eV for Cl[16], and 11,8 eV for Br[17]. While Br can be quantitatively measured to some extent, Cl is extremely difficult, and F cannot be determined using ICP-MS at all (at least in positive mode)[13]. Some examples for other methods that are currently being developed for F include Combustion Ion Chromatography (CIC), Instrumental Neutron Activation Analysis (INAA), or Particle-Induced Gamma Emission (PIGE), though techniques like PIGE require complex and expensive instrumentation and are therefore not viable for standard laboratories[18]. Most remaining methods require liquid samples obtained through digestion leading to systematic errors caused by sample preparation as well as longer analysis duration, which is undesirable. So, considering that there is currently no suitable method available, there is need for the development of one.

The method used in this work, possessing advantages over all previously mentioned techniques, is called Laser Induced Breakdown Spectroscopy (LIBS). It offers access to spatial resolution (imaging and depth profiling), fast measurements with limited sample preparation, straightforward instrumentation, and can theoretically detect all elements. The disadvantages, however, are low excitation efficiencies for some elements[19] resulting in difficult quantification and high limits of detection (LOD), a strong dependence on the laser energy, and the occurrence of matrix effects requiring matrix-matched standards. Furthermore, both Cl and Br exhibit their most intense emission lines in the UV region[14], which is not always accessible. Consequently, less intense emission lines must be employed, further complicating quantification. Therefore, to provide quantitative measurements in the µg/g range, the signal intensities of some elements, like the halogens, need to be improved. To achieve this for F, the latest research for instance utilizes the recombination of F with Ca or Cu and measurement of CaF or CuF molecular emission bands to increase sensitivity[19,20]. This, in turn, leads to more laborious sample preparation.

The novelty of this work is the use of LIBS under reduced pressure to improve the signals of F, Cl, and Br in polymer coatings. This could theoretically lead to enhancements regarding the sensitivity of these elements based on changing plasma dynamics. As the

expansion of the LIBS plasma plume at reduced pressures leads to less plasma shielding, which in turn leads to more ablation and less peak broadening, the resolution and signal-to-noise ratio (SNR) can be increased drastically. This could be used for better quantification, provided that the light collection optics have a field of view that encompasses the geometry of the plume accordingly. The aim of this thesis is ultimately the development of a method that is able to perform LIBS experiments under reduced pressure and allows for the fast quantification of F, Cl, and Br in the µg/g range.[21]

2 Theoretical Background

The following section aims to briefly explain the theory behind the used techniques. Of course there are many different types of lasers, light collection systems, spectrometers, and data processing methods, but the focus shall lie on the equipment relevant to this work. This is why, for instance, only the Nd:YAG laser will be explained.

2.1 Laser Induced Breakdown Spectroscopy (LIBS)

In Laser Induced Breakdown Spectroscopy (LIBS) the surface of a sample is irradiated with a laser. By absorbing the energy provided by the laser, a small part of the material is ablated and vaporized, forming a plasma. To enhance the ablation and ensure a suitable atmosphere, the sample chamber is usually flushed with He or Ar although operation under atmospheric conditions is also possible. The vaporized particles further interact with the laser leading to atomization, excitation, and ionization of the generated species. Relaxation of these excited atoms, ions, and simple molecules in the plasma then leads to the emission of characteristic radiation. The spatial propagation of the plasma plume is subject to plasma dynamics and dependent on many different variables, like pressure, temperature, and atmosphere, making it a very complicated matter. A portion of the emitted plasma light is then collected by a light collection system, for instance a fiber optic cable or light collection optics, and transferred to a spectrometer. The spectrometer disperses the polychromatic light and a detector, often a CCD camera, records the LIBS spectrum containing characteristic atomic and ionic emission lines, as well as molecular bands. Finally, this spectroscopic information enables qualitative and quantitative analysis. A schematic of the usual LIBS instrumentation showcasing the working principle is depicted in Figure 1.[22]

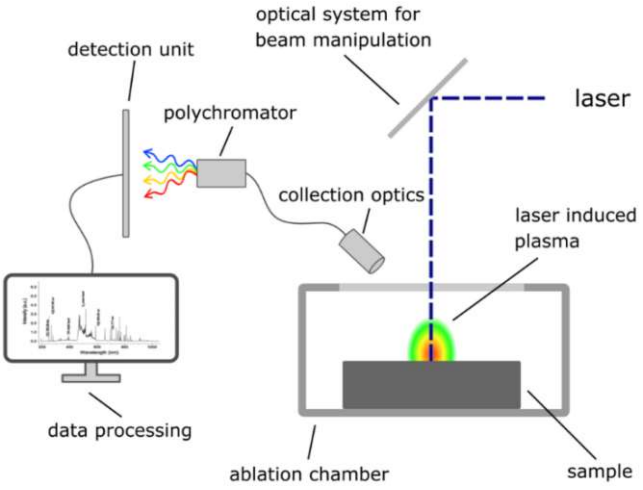

Figure 1: Schematic of the LIBS working principle and required instrumentation. The sample surface is irradiated with a laser and a plasma is formed. The emitted plasma radiation is then captured and transferred to a spectrometer for subsequent analysis providing qualitative and quantitative information.[23]

LIBS is a unique technique in the field of direct solid sampling elemental analysis and the main advantages are[22–25]:

- it is theoretically able to detect all elements of the periodic table
- limits of detection (LOD) ranging to the µg/g level
- LIBS offers simultaneous multi-element analysis making it an excellent tool for non-targeted analysis, which is very valuable for sample classification based on elemental fingerprint
- it provides spatially resolved measurements with a lateral resolution in the lower µm range and a depth resolution of a few hundred nm enabling fast imaging as well as depth profiles
- virtually no sample preparation needed apart from ensuring that the specimen fits inside the ablation chamber, which also reduces the experiment duration
- only a small amount of sample required for analysis
- LIBS experiments can be performed in a stand-off configuration
- relatively simple instrumentation

Like any other method, however, LIBS also has some disadvantages:

- some elements (like F, Cl, and Br) require high excitation energies, which leads to low intensity emissions making quantification difficult[26]
- LIBS suffers severely from matrix effects requiring matrix-matched standards (standards with fairly similar chemical and physical properties as the sample) to perform quantitative analysis[25]
- a strong dependance on laser energy further complicating quantification, though this can be compensated to some extent by normalizing the acquired data

2.2 Laser

The term ‘laser’ is an acronym for Light Amplification by Stimulated Emission of Radiation. To understand lasers, it is important to understand the stimulated emission of radiation. When an atom or molecule absorbs a photon with suitable energy, it can be raised from its ground state with energy E_1 to an excited state with energy E_2. This process is called absorption and is illustrated in Figure 2c. As $E_2 > E_1$ the system will undergo a relaxation back to its ground state during which the energy difference is released. If the energy difference is released in the form of electromagnetic radiation, which is called radiative decay, there are two possibilities for it: spontaneous emission and stimulated emission. The spontaneous emission, which is dependent on the lifetime of the state and depicted in Figure 2a, is characterized by the emission of one photon with energy $E_2 - E_1$ without any external stimulus. Stimulated emission on the other hand occurs when an incident

photon with the exact same energy of $E_2 - E_1$ interacts with the excited atom/molecule. In this case, there is the possibility that the incident photon forces the atom/molecule to undergo the relaxation resulting in the emission of two photons with the same energy $E_2 - E_1$. This process, which is illustrated in Figure 2b, differs fundamentally from the spontaneous emission and results in the two photons having the exact same direction and phase. The ability to amplify light in this way is the basic operation principle of a laser.[27]

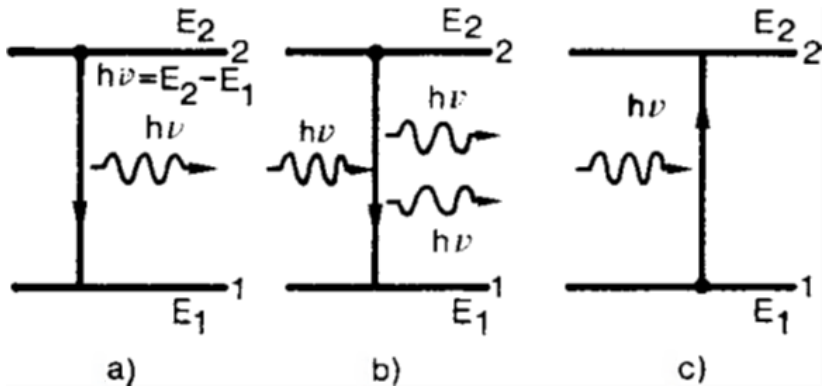

Figure 2: Schematic illustration of a) spontaneous emission, b) stimulated emission, and c) absorption. Stimulated emission is the basis of a laser.[27]

Nd:YAG lasers are the most popular type of solid-state lasers. In them a $Y_3Al_5O_{12}$ crystal (referred to as YAG, an acronym for yttrium aluminum garnet) doped with Nd acts as the active medium in which a population inversion is achieved. At a typical doping level of 1 at.% some Y^{3+} ions are replaced by Nd^{3+} which leads to the usually transparent host material becoming pale purple and acquiring desirable optical properties. Nd:YAG is typically used in form of a rod with a diameter between 3 and 6 mm and a length between 5 and 15 cm.[27]

A simplified energy scheme of Nd:YAG can be seen in Figure 3a, the pumping scheme of a four-level laser in Figure 3b, and the working principle of a Nd:YAG laser is as follows. Initially, the light from a flash lamp is exciting the active medium Nd:YAG from its ground state $^4I_{9/2}$ to a pumping level, for instance $^4F_{5/2}$, which is termed optical pumping. After this, a nonradiative decay to the metastable $^4F_{3/2}$ level takes place, which is faster than the initial excitation. From there, a relaxation from $^4F_{3/2}$ to $^4I_{11/2}$ results in the emission of a photon with 1064 nm wavelength, the main emission line of a Nd:YAG laser. In the end, another fast nonradiative decay from $^4I_{11/2}$ to $^4I_{9/2}$ ensures that thermal equilibrium between the two states is established. Because the energy difference between $^4I_{11/2}$ and $^4I_{9/2}$ is greater than kT, the upper $^4I_{11/2}$ level can be considered empty according to Boltzmann statistics. A Nd:YAG laser has four energy levels participating in the process and is therefore called a four-level laser. As the nonradiative transitions from $^4F_{5/2}$ to $^4F_{3/2}$ and $^4I_{11/2}$ to $^4I_{9/2}$ are much faster than the radiative ones and optical pumping ensures

continuous excitation a population inversion is achieved. This means that the upper level $^4F_{3/2}$ is more occupied than the lower level $^4I_{9/2}$, which is essential for light amplification by stimulated emission of radiation.[27]

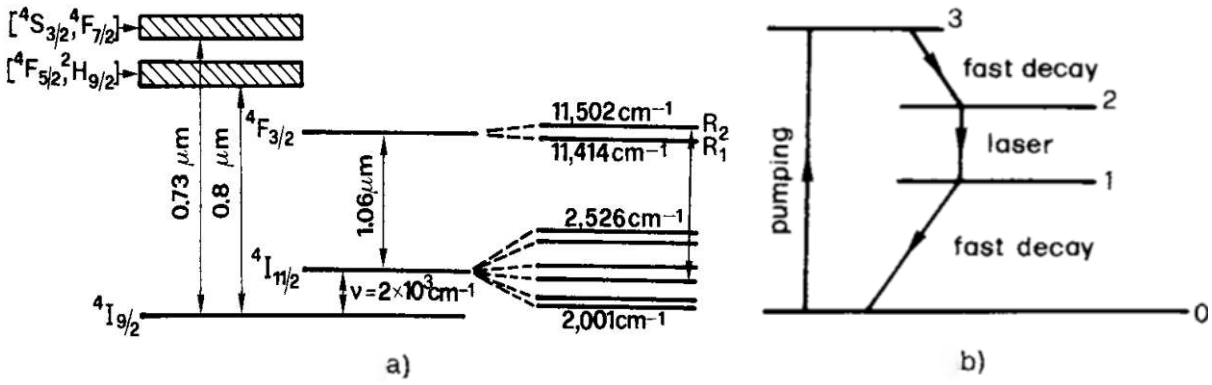

Figure 3: a) Simplified energy levels of Nd:YAG. The main laser emission with a wavelength of 1064 nm results from the $^4F_{3/2}$ to $^4I_{11/2}$ transition. b) Pumping scheme of a four-level laser.[27]

The three main components of a solid-state laser are shown in Figure 4: the optically active medium (Nd:YAG), the pumping system (flash lamp), and a resonator structure (two mirrors). When photons with a wavelength of 1064 nm are emitted by the Nd:YAG and travel along the axis of the cavity, they are reflected by the mirrors and continuously interact with the Nd:YAG resulting in ever increasing stimulated emission of radiation. This leads to amplified laser radiation consisting of many photons with the same wavelength, direction, and phase exiting the laser through the partially reflecting mirror. Finally, the generated laser beam is characterized by a high degree of monochromaticity, coherence, directionality, brightness, and the capability of producing very short light pulses. It is possible to change the laser wavelength to e.g. 266 nm through optical frequency multiplication.[27]

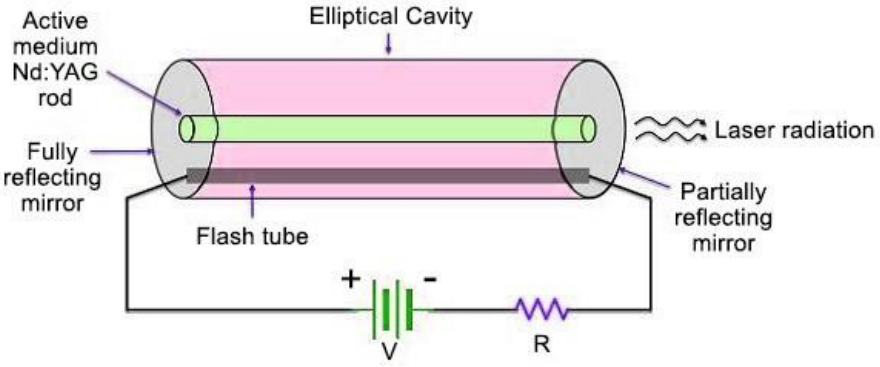

Figure 4: The three main components of a Nd:YAG laser are the active medium (Nd:YAG), the pumping system (flash lamp), and a resonator structure (two mirrors, one partially reflecting).[28]

2.3 Effects of reduced pressure and atmospheric composition on LIBS

The pressure inside the ablation chamber has a big impact on the observed LIBS spectrum and changing it can therefore significantly improve the signal intensity, spectral line width, and signal-to-noise ratio. However, as the formation of the plasma and the resulting signal is a very complex process and dependent on many variables (e.g. pressure, buffer gas, laser energy, type of laser, investigated element, ...), it is difficult to determine the exact effect that a change in pressure will exert on a LIBS spectrum, and there are even contradicting statements found in literature. One effect that reduced pressure can have on a spectrum is increased emission line intensity, which can be explained by prolonged plasma lifetime. During the expansion of the plasma, after the initial ablation, the plasma loses energy to the surrounding atmosphere, leading to a shortened plasma lifetime and subsequently less emitted radiation. Therefore, reducing the pressure in the ablation chamber results in a less dense atmosphere, less energy losses, a longer plasma lifetime, more emitted plasma radiation, and finally higher intensity. If the pressure is too low, however, a lack of sufficient plasma confinement leads to diminished excitation and, as in the beginning, less intensity.[21,29]

Another factor that must be considered is the ablated area. In a less dense atmosphere, the shock wave generated by laser irradiance will also be less dense, resulting in decreased plasma shielding, which allows for more photons to reach the sample surface. This subsequently increases the ablated area and the overall signal intensity.[21,30]

Furthermore, the impact of the atmospheric composition must also be considered when designing LIBS experiments. Ar plasmas exhibit higher electron densities compared to He, as Ar possesses a lower ionization energy, which leads to enhanced line broadening and therefore decreased resolution. So while Ar generally leads to higher intensity, a better signal quality can be obtained in He atmosphere.[21]

As all these effects will influence the shape of the expanding plasma plume, operating a light collection system with a suitable field of view, that encompasses the plasma geometry, is crucial. Figure 5 illustrates the significant impact that reduced pressure can have on a LIBS plasma plume.[21]

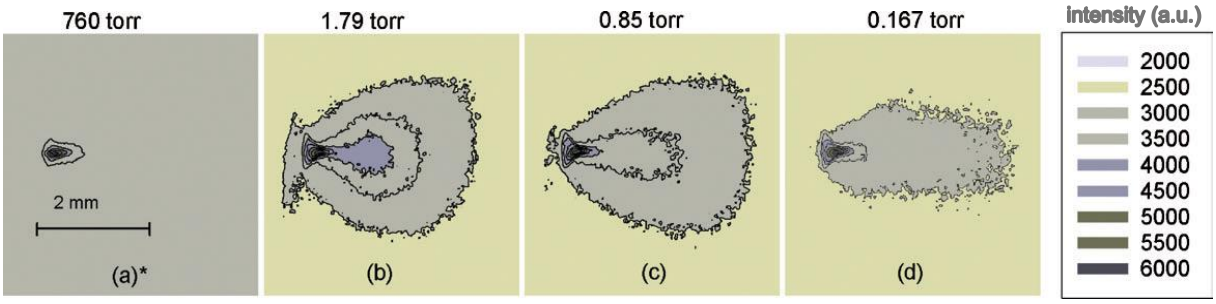

Figure 5: Two-dimensional plasma plume images of a Cu plasma at different pressures. Reduced pressure leads to a plasma plume expansion, adapted from Yalçın et al.[31].

2.4 Light collection system

The light collection system is the optical equipment responsible for gathering the emitted plasma radiation and transmitting it to the spectrometer for subsequent analysis. It can either be an image formation system, for instance a lens, or an optical fiber usually positioned close to the plasma plume.[21]

2.4.1 Collection optics

A system of lenses that captures the emitted plasma radiation is called collection optics. Collection optics are usually placed a few centimeters away from the plasma plume as to receive radiation coming from the entire plasma plume and to minimize its fluctuations in position, morphology, electronic temperature, and density. This way, it is also possible to survey a larger sample area which is beneficial for imaging. Nonetheless, a correct alignment of the optics is essential. The collected plasma light is then transmitted to a spectrometer using a fiber optic cable. A typical installation of collection optics with connected fiber optic cables is shown in Figure 6.[21,32,33]

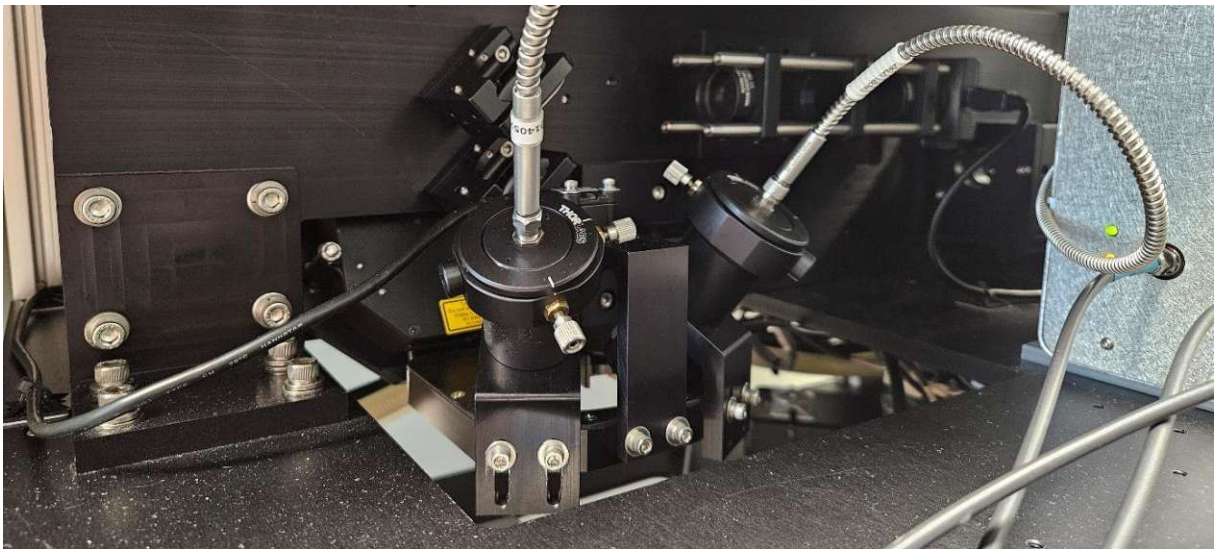

Figure 6: The collection optics of the J200 LIBS instrument (Applied Spectra, Inc., West Sacramento, USA). A system of lenses captures the emitted plasma radiation which is then transferred to the spectrometer via a fiber optic cable.

2.4.2 Fiber optic cable

In contrast to the collection optics, it is also possible to capture the emitted plasma light directly next to the plasma plume using a fiber optic cable whose structure can be seen in Figure 7a. A fiber optic cable transmits light with high efficiency using total internal reflection provided that the light rays enter the fiber within the numerical aperture. As a result, the view sight of an optical fiber is restricted to an acceptance cone defined by the

numerical aperture so that only the radiation with an incident angle smaller than the cone angle is collected. For a fused silica optic fiber this acceptance angle is typically ~26 °, as illustrated in Figure 7b. Because of this restricted acceptance angle, the precise alignment of the fiber with regard to the plasma plume, usually at a distance of ~1 cm, is even more crucial than for collection optics in LIBS experiments. This applies in particular for light collection under reduced pressure where the plasma plume propagates even faster.[22,33]

In this work, the use of a fiber optic cable as the light collection system is also referred to as 'direct sampling'.

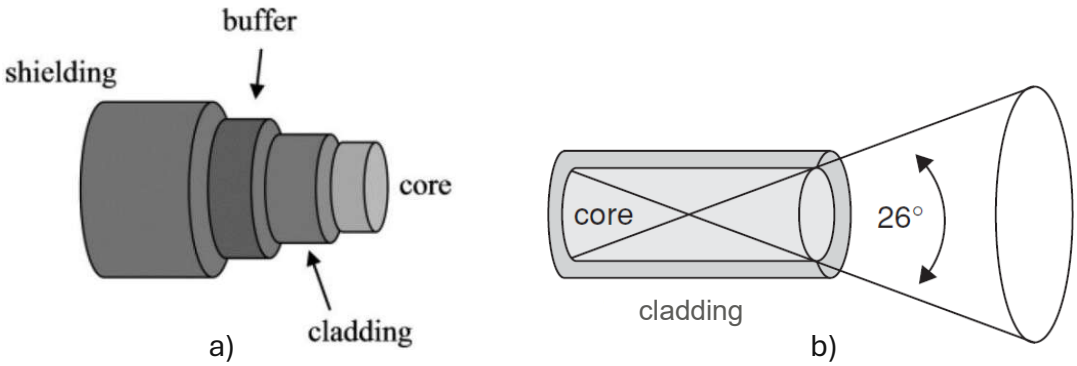

Figure 7: a) Structure of a fiber optic cable and b) acceptance angle of typically ~26 ° for fused silica optic fibers resulting in a restricted field of view. A proper placement of the fiber optic cable is crucial in LIBS experiments.[22]

2.5 Spectrometer

A spectrometer consists of a spectrograph, responsible for separating the incoming light by its wavelengths, and a detector, which collects and records the separated spectrum. Ideally, a spectrometer should have a wide wavelength range, high spectral resolution, large dynamic range, and short readout and data-acquisition time. In practice, however, a tradeoff must always be made when designing LIBS experiments and selecting the most convenient spectrometer combination, especially when the spectral range, sensitivity and cost are considered. In LIBS, a broadband spectrometer (Czerny-Turner spectrograph and CCD detector for each channel) providing a wide wavelength range (e.g. 200–1000 nm) is a popular option, as it enables the measurement of multiple emission lines albeit with lower resolution. For the precise, high resolution determination of a narrower spectral range, a Czerny-Turner spectrograph utilizing a ICCD (Intensified Charge Coupled Device) detector is a good choice.[21,22]

In a Czerny-Turner spectrometer, which is diagrammed in Figure 8, the incoming plasma radiation passes through the entrance slit and is then intercepted by a spherical mirror. This first mirror collimates the incident light and reflects it onto a plane diffraction grating, which spatially disperses the spectral components. Resulting from the diffraction, each

spectral component exits the grating propagating in a slightly different angular direction. A second spherical mirror is then collecting and focusing the spectral components onto a detector in different spatial positions. Because of their design and the limited space on a ICCD chip, Czerny-Turner spectrometers utilizing ICCD detectors are restricted either in resolution or spectral coverage. This means, that they can cover a narrow spectral range with higher resolution, or a wide spectral range with lower resolution.[21,22]

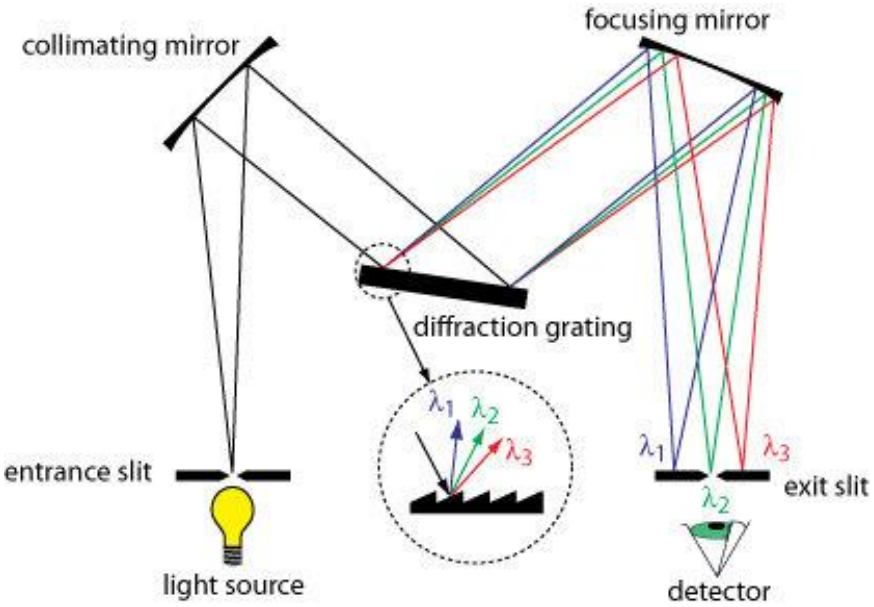

Figure 8: Schematic of a Czerny-Turner spectrometer, which utilizes a diffraction grating to disperse the incoming radiation.[34]

In the context of a spectrometer, the gate delay (GD) and the gate width (GW) are important parameters. The gate delay indicates the time that elapses between the firing of the laser and the start of the recording by the detector. The gate width is comparable to the exposure time in photography, as it indicates the duration for which the detector records. In the LIBS experiments conducted in this work, both are typically in the lower µs range.

2.6 Normalization in LIBS

Since the intensities in the resulting LIBS spectrum are strongly dependent on the laser energy and plasma properties, as already mentioned in section 2.1, a normalization of the signals is necessary to reduce signal fluctuations, of the peak as well as the background, and make the measurements comparable. In LIBS, a normalization generally tries to establish a connection to the plasma properties. The right type of normalization in LIBS is still an unanswered question today and unfortunately there is no one-fits-all solution. The

best type must be found for each element and sample by testing different kinds of normalizations. To achieve the right kind of normalization for halogens in polymer coatings, the guidelines set by Guezenoc et al. were followed in this work. An overview of the investigated types, all of them mathematical transformations of the raw data where the analyte signal is divided by another signal like the background, which is an indicator of the plasma properties, is given in the following section.[35]

Of course, there is also the possibility of applying no normalization to the intensity or the area of a peak. The effects of this on quantitative LIBS experiments will be discussed in the results.

To illustrate the general data processing of emission lines, a schematic of a peak with applied linear background correction is depicted in Figure 9. To determine the background intensity value in the vicinity of the peak, a Python script applying a linear background correction was used. This background intensity value was then used for the normalization to the background (BG), which is explained in detail in the following section 2.6.1, and all normalizations employing peak areas used background corrected peak areas (area below the peak subtracted).

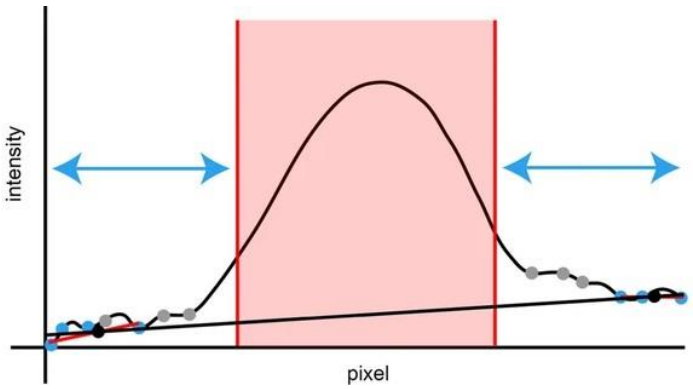

Figure 9: Schematic illustration of the linear background correction used to determine the background intensity value in the vicinity of the peak.[36]

2.6.1 Background (BG)

In normalization to the background the peak intensity value of the analyte's emission line is divided by the intensity value of the background emission in the vicinity to it. Ideally, the intensity value of the background emission is recorded over a spectral window and then averaged as opposed to recording one intensity value at a single wavelength. In this case, normalization to the background is equal to the signal-to-background ratio (SBR). The background normalized intensity is calculated according to the following Equation 1.[35]

$$I_{BG\ normalized} = SBR = \frac{I_{Peak}}{I_{BG}} \quad (1)$$

$I_{BG\ normalized}$.... background normalized intensity
SBR ..... signal-to-background ratio
I_{Peak} ..... intensity of the analyte peak
I_{BG} ..... intensity of the background

Normalization to the background works especially well because continuum radiation, like the background, is a good indicator of plasma properties such as its density.[37] Therefore, it is one of the most widely used normalization concepts in LIBS and has been successfully applied to various problems.[38–40]

2.6.2 Internal Standard (IS)

In normalization to an internal standard the peak intensity value of the analyte's emission line is divided by the peak intensity value of an internal standard's emission line. The same can be done for the areas of the peaks. Ideally, the concentration of the internal standard is known and remains constant for all standards of the calibration. The internal standard normalized intensity or area is calculated according to the following Equation 2.[35]

$$I_{IS\ normalized} = \frac{I_{Peak}}{I_{IS}} \quad \text{or} \quad A_{IS\ normalized} = \frac{A_{Peak}}{A_{IS}} \quad (2)$$

$I_{IS\ normalized}$ .... internal standard normalized intensity
I_{Peak} ..... intensity of the analyte peak
I_{IS} ..... intensity of the internal standard peak
$A_{IS\ normalized}$ ... internal standard normalized area
A_{Peak} ..... area of the analyte peak
A_{IS} ..... area of the internal standard peak

Although the internal standard method is widely used in other analytical techniques, it is very difficult to perform in LIBS. Some sources even claim that it is almost impossible to apply it correctly.[41] The reason for this are the strict requirements an internal standard must fulfill to ensure that the method works properly. For example, the analyte and the internal standard should have: similar volatilization rates, ionization energies, atomic weights, spectral line excitation energies, spectral line intensities, and the spectral lines should not exhibit self-absorption.[41,42]

Since these criteria often cannot be fulfilled while performing LIBS experiments the internal standard normalization is not widely used and is reserved for specific cases.[35]

2.6.3 Total Area (TA)

In normalization to the total area the peak intensity value of the analyte's emission line is divided by the sum of all the intensity levels of the entire spectrum. The better the resolution of the spectrometer the more accurate this sum can be calculated. The total area normalized intensity is calculated according to the following Equation 3.[35]

$$I_{TA\ normalized} = \frac{I_{Peak}}{I_{TA}} = \frac{I_{Peak}}{\sum I_i} \tag{3}$$

$I_{TA\ normalized}$.... total area normalized intensity
I_{Peak} ..... intensity of the analyte peak
I_{TA} ..... sum of the intensities of the entire spectrum (= total area)
I_i ..... intensity at a single wavelength

Normalization to the total area works well because the intensity of the entire spectrum is a good indicator of the laser energy and subsequently the plasma properties, just like the background.[43] Therefore, it is also a popular normalization method in LIBS and one of its most well-known uses is the normalization of data provided by the ChemCam (a LIBS device) onboard NASAs mars rover curiosity.[35,44]

2.6.4 Subtraction (SUB)

Normalization via subtraction is a concept similar to the internal standard with regard to utilizing a constant peak somewhere else in the spectrum. The underlying background of the analyte's emission line peak area is subtracted by calculating the ratio of this background to a constant peak in the vicinity (normalization peak) for the blank measurement and then multiplying this ratio with the normalization peak for each concentration. This works under the assumption that the ratio remains constant. This concept can be better understood by looking at the following example of an analyte peak at 685 nm with a normalization peak (e.g. an internal standard) at 688 nm which is given in Equation 4.

$$A_{A685} = A_{685} - A_{BG685} = A_{685} - r \cdot A_{688} = A_{685} - \frac{A_{BG685,blank}}{A_{688,blank}} \cdot A_{688} \quad (4)$$

A_{A685} ..... area of the analyte peak at 685 nm
A_{685} ..... area of the entire peak at 685 nm
A_{BG685} ..... area of the background at 685 nm
r ..... ratio of the background at 685 nm and the normalization peak at 688 nm for the blank measurement
A_{688} ..... area of the entire peak at 688 nm
$A_{BG685,blank}$ .... area of the background at 685 nm for the blank measurement
$A_{688,blank}$ ..... area of the entire peak at 688 nm for the blank measurement

2.7 Analytical figures of merit

The following section aims to give a brief description of the most important analytical figures of merit used in this work.

2.7.1 Limit of detection (LOD)

According to IUPAC the limit of detection (LOD) is the smallest concentration of analyte in a sample that can be reliably distinguished from zero. Although the definition is very concise the calculation in LIBS is not as clear and there are different approaches, like the blank method, where three times the standard deviation of the blank measurement is divided by the slope of the calibration curve. One possibility, which is handy when working with calibrations, is the determination based on the standard error of the estimate that can be calculated from the calibration curve. The LOD should not be confused with the limit of quantification (LOQ). In this work the LOD is calculated according to the following Equation 5.[45]

$$LOD = \frac{3{,}3 \cdot S_Y}{b} \quad (5)$$

LOD ..... limit of detection
S_Y ..... standard error of the estimate (as standard deviation of the response)
b ..... slope of the linear calibration curve

2.7.2 Root mean square error (RMSE)

Once a quantitative model, such as a calibration curve, is built, it provides the ability to predict concentration values, and a figure of merit based on the prediction error can be defined. In addition to the coefficient of determination (R^2) the root mean square error (RMSE) compares the predicted concentration values of the model to the known reference concentration values and determines the prediction ability. It has the same concentration unit as the samples and should be as low as possible for a reliable model. However, it should be noted that the higher concentration values have a greater influence on the RMSE value. The RMSE is calculated according to the following Equation 6.[35,46]

$$\mathrm{RMSE} = \sqrt{\frac{\sum_{i=1}^{N}(c_i - \hat{c}_i)^2}{N}} \tag{6}$$

RMSE..... root mean square error
N..... number of samples
c_i ..... predicted concentration values
$\hat{c}_i$ ..... reference concentration values

3 Experimental

3.1 LIBS System

3.1.1 Laser

The device used for this work was the J200 LIBS instrument (Applied Spectra, Inc., West Sacramento, USA) which had a Nd:YAG laser with a wavelength of 266 nm and a pulse duration of 6 ns. It was able to reach a fluence of up to 8 J/cm^2 measured at the sample surface, operated with a frequency of 20 Hz, and had a circular beam shape. The spotsize (size of the beam) could be adjusted but was used at a constant diameter of 100 µm for all experiments. Either helium and/or argon could be chosen as gas flow into the ablation chamber, which was mounted onto a moveable stage providing accurate placement of ablation patterns. The fiber optic cable of the spectrometer was connected to the collection optics which were placed in the top of the device about 20 cm away from the ablation chamber. Essentially consisting of several lenses, these collection optics captured the emitted radiation during experiments and were the installed standard equipment in this device. The system, see Figure 10, was controlled using the software Axiom 2.0 (Applied Spectra, Inc., West Sacramento, USA).

Figure 10: The J200 LIBS instrument (Applied Spectra, Inc., West Sacramento, USA) equipped with a 266 nm Nd:YAG laser used for this work.[47]

3.1.2 Spectrometer

The spectrometer SpectraPro HRS-750 equipped with a Schmidt-Czerny-Turner spectrograph (reduces optical aberrations) and ICCD camera PI MAX 4 (Teledyne Princeton Instruments, Trenton, USA), see Figure 11, was used to analyze the emitted

radiation and provide high resolution spectra. Due to the low intensity of halogen emission lines the ICCD camera and its ability to intensify already weak signals was particularly useful. The emission lines utilized for the analysis of the target elements were F I 685,6 nm, Cl I 837,6 nm, and Br I 827,3 nm. At the beginning of each experiment the optic fiber cable entering the spectrometer had to be positioned in a specific way, as to maximize the incoming radiation. This so-called 'instrument tuning' was accomplished by measuring the NIST® Standard Reference Material® 612 (National Institute of Standards and Technology, Gaithersburg, USA) with standardized laser settings and monitoring the unidentified 458 nm emission line. The intensity of this signal was maximized by turning the fiber optic cable until its exit slit was in the optimal position. The instrument tuning had to be performed after any movement of the fiber optic cable or change in experimental setup. All experiment parameters had to be optimized to achieve quantitative results in the µg/g range, the exact parameters for each measurement will be given in the results section.

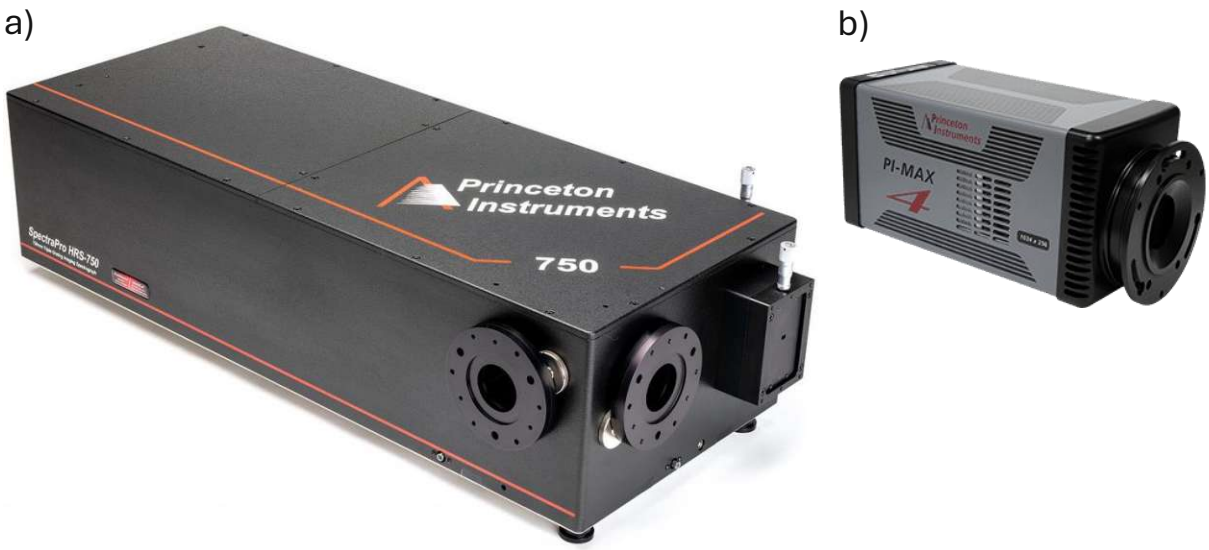

Figure 11: a) Spectrometer SpectraPro HRS-750[48] with b) ICCD camera PI MAX 4[49] (Teledyne Princeton Instruments, Trenton, USA).

The spectrometer was controlled using the software LightField® (Teledyne Princeton Instruments, Trenton, USA) with which accumulated spectra could be averaged automatically. This proved to be especially useful when conducting line scans since it is custom in LIBS to average spectra over larger sample areas to achieve more representative results.

3.1.3 Heating Stage (HS)

The name of this stage stems from a former project and although the influence of other parameters such as temperature and voltage could be investigated using this device, the use of vacuum was the main focus of this work. Nevertheless, it will be referred to as 'heating stage' (HS) hereafter.

The HS, see Figure 12, was used to perform LIBS experiments under reduced pressure. To achieve this, one of the push-in fittings built into the ablation chamber was connected to a laboratory vacuum pump ILMVAC LVS 110 Tp ecoflex (ILMVAC GmbH, Ilmenau, Germany) and the other one to the gas supply of the J200 providing He as well as Ar. This way, the ablation chamber containing the sample could be flushed continuously with He and/or Ar while maintaining reduced pressure. A typical gas flow during measurements without vacuum was 1 L/min while the flow had to be decreased to ca. 0,2 L/min for the pump to reach a pressure of 50 mbar.

When using the HS, the emitted radiation was captured by the collection optics of the J200. Since these were mounted in the top right rear of the J200, the samples had to be placed slightly left below the center of the ablation chamber to avoid the top plate blocking the plasma emissions from entering the collection optics. Conveniently, the HS ablation chamber offered enough space to accommodate four wafers at a time which enabled efficient measurements. The custom-made ablation chamber was glued to a 3D printed mount (white component in Figure 12) and then screwed onto the moveable J200 stage.

Figure 12: Using the heating stage (HS), LIBS experiments could be performed under reduced pressure with collection optics sampling.

3.1.4 Development of the Direct Stage (DS)

An alternative way of sampling the emitted radiation was to place the entrance of the fiber optic cable inside the ablation chamber as opposed to connecting it to the collection optics located about 20 cm away from the plasma. This should theoretically lead to higher collection efficiency and subsequently more intense signals since the emissions are not forced to pass through the cover glass of the ablation chamber and travel to the collection optics in atmospheric conditions. To facilitate this method of sampling and combine it with the ability to perform measurements under reduced pressure, a hole was drilled into the wall of an ablation chamber, which was custom-built in-house, and a thread was fitted into it so that the fiber optic cable could be screwed on. This way, the plasma emissions could be captured directly next to the sample, hence the name 'direct sampling stage' or in short 'direct stage' (DS).

To provide vacuum, two opposing openings were equipped with push-in fittings Festo QSM-M5-4 (Festo Corporation, Islandia, USA) and connected to vacuum pump and J200 gas supply as for the HS in section 3.1.3.[50]

The ablation chamber was then pressed into the 3D printed chamber mount which can be seen in Figure 13b. By 3D printing the recesses with an accuracy of 0,2 mm the ablation chamber was firmly held in place by the chamber mount without the need for any screws. The chamber mount (Figure 13d) was then bolted onto the base plate (Figure 13c), which was also 3D printed, using four M3 screws. The assembled DS could then be mounted into the J200, as depicted in Figure 13e, providing LIBS experiments under reduced pressure as well as utilizing direct sampling.

Due to the huge influence of the sample position on the resulting signal intensities, spacers with practical shape and different heights were 3D printed to achieve optimal sample height in the chamber. These can be seen in Figure 13a next to the stained cover glass or in Figure 13b placed in the ablation chamber.

All 3D printed parts were designed using the CAD software Autodesk Fusion 360 (Autodesk, Inc., San Rafael, USA), which provided a quick and easy solution, and printed in-house.

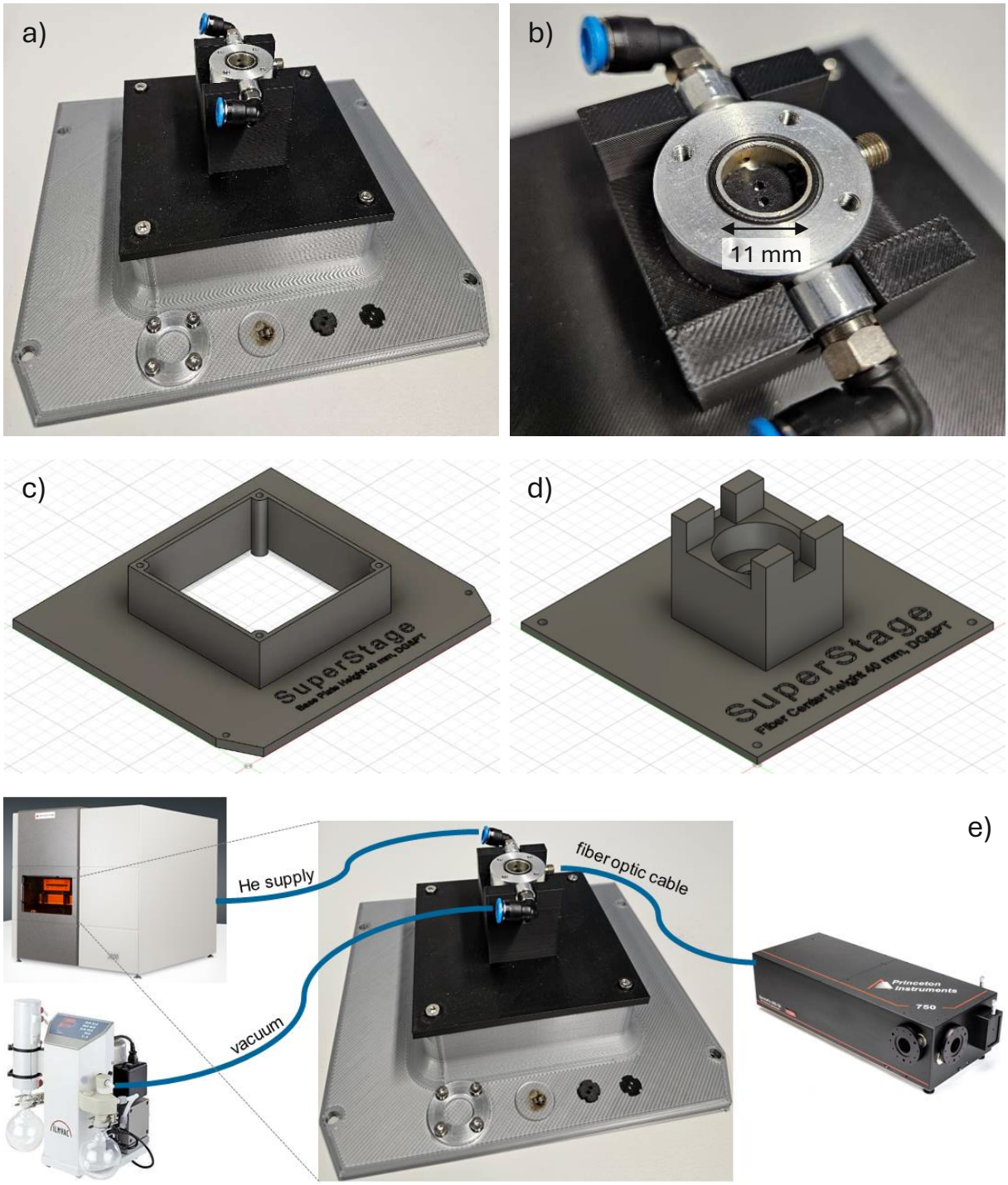

Figure 13: Development of the Direct Stage (DS): a) assembled DS with cover glass and 3D printed spacers, b) ablation chamber with push-in fittings and fiber optical cable thread firmly held in place by chamber mount without the need for screws, c) CAD drawings for the base plate and d) chamber mount, and e) fully assembled LIBS system with DS connected to J200[47], which provided a 266 nm Nd:YAG laser and He/Ar gas supply, vacuum pump[51], and spectrometer[48]. The sample in the chamber was ablated by the laser in vacuum and He/Ar atmosphere and the plasma emissions captured by the fiber optic cable with subsequent analysis using the spectrometer. To summarize, this experimental setup enabled LIBS experiments under reduced pressure while utilizing direct sampling.

3.1.5 Ablation pattern

There were three ablation patterns available in Axiom 2.0, the software with which the J200 was controlled[52]:

- Spots: The laser fires the set number of shots on one spot and then moves on to the next spot until the pattern is finished.
- Lines: The laser is positioned at the beginning of the line and starts firing continuously as it is moved along the line at a set velocity until the end is reached. It then moves on to the next line until the pattern is finished.
- Raster: The raster is similar to a parallel line pattern except that the lines are connected to form a snake pattern, and the laser is continuously firing throughout the pattern.

3.2 Preparation of standards

To perform a calibration, which allows quantitative measurements, samples with known concentrations were needed. These standards, polyimide coatings doped with different halogen contents, were prepared using in-house materials. All chemicals used for this process are listed in the following Table 1 as well as the instruments in Table 2.

Table 1: Chemicals used for standard preparation.

Name	Supplier	Information
Polyimide powder P84 (PI)	Ensinger Sintimid GmbH, Lenzing, Austria	200 mesh
N-Methyl-2-pyrrolidone (NMP)	Merck KGaA, Darmstadt, Germany	p.a.
2-Amino-4,5-difluorobenzoic acid	Fluorochem, Hadfield, UK	
4-Chlorobenzoic acid	Merck KGaA, Darmstadt, Germany	99 %
4-Bromobenzoic acid	BLD Pharmatech GmbH, Reinbek, Germany	97,48 %
Silicon wafers	Infineon Austria AG, Villach, Austria	10×10 mm^2
Aluminium foil	Merck KGaA, Darmstadt, Germany	high purity

Table 2: Instruments used for standard preparation.

Name	Supplier
Analytical balance ENTRIS® II BCE224I-1S	Sartorius, Göttingen, Germany
Vortex-Genie 2	Scientific Industries Inc., Bohemia, USA
Ultrasonic Cleaner USC200TH	VWR, Radnor, USA
FluoroPlate heating plate	Analab, Hoenheim, France

To prepare the standards polyimide powder was dissolved in NMP, which required the use of a vortex and ultrasonic bath, to obtain a 10 wt.% solution of PI in NMP. To introduce

halogens as dopants, the halogenated organic substances 2-Amino-4,5-difluorobenzoic acid, 4-Chlorobenzoic acid, and 4-Bromobenzoic acid were also dissolved in NMP, which is an organic solvent. These solutions were carefully homogenized and then further diluted with NMP to obtain the desired halogen concentrations. Standard solutions were then prepared by spiking the 10 wt.% PI/NMP solution with the halogen solutions. To form a solid layer of halogen-containing polymer coating 75 µL of the standard solutions were applied onto Si wafers or Al foil and distributed as evenly as possible. The solvent was then evaporated using a heating plate at 120 °C for 1 h. After letting the standards slowly cool down to room temperature by simply turning off the heating plate, solid PI layers containing defined amounts of halogenated compounds had formed on top of the wafer/foil. In some cases, the temperature ramp of the heating plate was too high which resulted in blisters forming while heating up and remaining cavities after cooling. These cavities could not be measured afterwards using LIBS and their formation should therefore be avoided.

Since the circular direct stage ablation chamber had a diameter of approximately 11 mm and the square Si wafers had a size of 10 × 10 mm^2 it was necessary to cut off the corners using pliers in order for the standards to fit inside the ablation chamber. This problem could be avoided using Al foil as a substrate, which could be cut to an octagonal shape with a diameter of 10 mm quite comfortably using scissors beforehand. During some measurements with the Si wafer standards, the polymer coating peeled off entirely and was reattached using double-sided adhesive tape. This problem did also not occur with the Al foil standards, presumably because of their rougher surface area and the resulting better adhesion of the PI coating.

The calculated halogen contents of the prepared standards, based on the weights of the prepared solutions, are listed in Table 3 and the resulting samples are depicted in Figure 14.

Table 3: Halogen contents of the prepared polyimide standards.

F content (µg/g)	Cl content (µg/g)	Br content (µg/g)
2172	9500	11117
1091	3321	3887
547	1014	2792
274	340	2333
110	102	1845
55	34	1381
27	10	1186
0	0	919
		481
		397
		119
		0

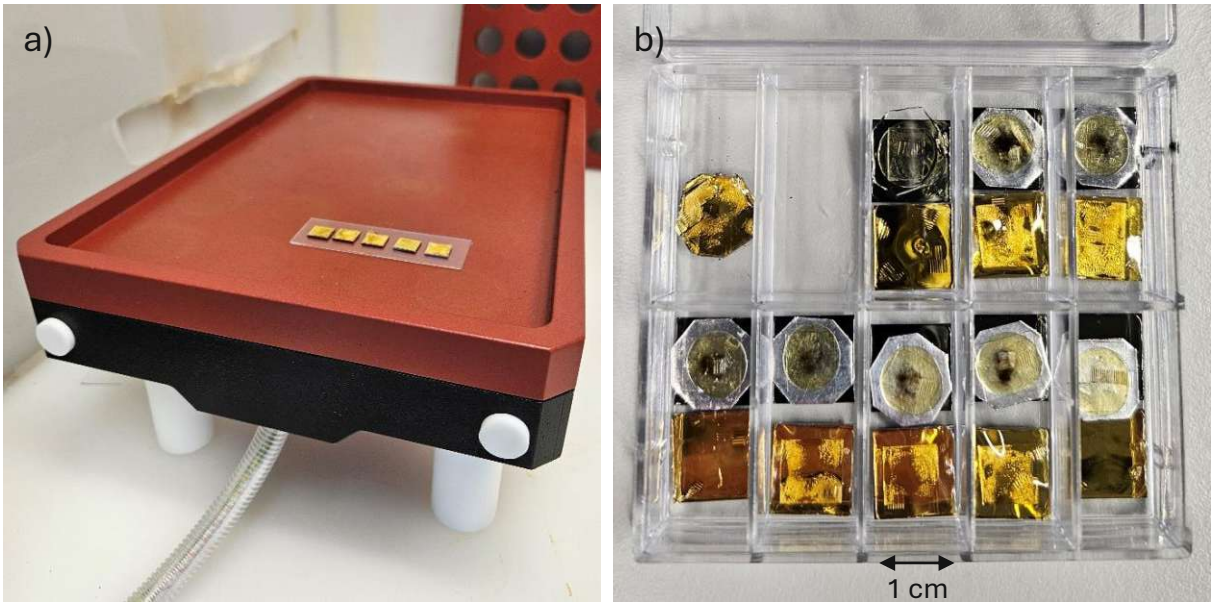

Figure 14: F standards a) during evaporation of NMP on a heating plate and b) as fully prepared samples using Si wafers as well as Al foil as a substrate. Already ablated areas appear as black spots, in some cases the shot pattern is visible.

4 Results & Discussion

This section aims to provide an overview of the results in chronological order. Before any quantitative analysis in the µg/g range could be attempted, a thorough optimization of every experimental parameter was necessary. This included the laser settings, atmosphere and placement of the standards in the ablation chamber, light collection system, as well as spectrometer configuration. However, in order to present the results concisely, only the most relevant parameters that are of particular importance for this work, such as the pressure in the ablation chamber, will be discussed. The optimized parameters for all investigated elements will be listed at the end of the respective subsections. During optimization, the standards with the highest concentrations were analyzed in order to detect changes in the spectra as clearly as possible. Finally, calibrations including all standards were measured applying these optimized parameters.

4.1 General optimization of the measuring procedure

4.1.1 Ablation pattern

Since the goal of these LIBS experiments was to achieve quantitative results in the µg/g range, the analyzed sample area had to be large enough to ensure representative results and a reliable measuring statistic. But since there was not an infinite number of standards available and the space in the ablation chamber which yielded signals with sufficient intensities was limited, the ablated area also needed to be small enough to allow feasible measurements. This problem was solved by choosing the right type of ablation pattern.

Spots were not suited for this task because the sampled area was too small as the spotsize (diameter of the laser beam) was usually 100 µm and changing positions between spots required a comparatively long time which resulted in inefficient measurements. This pattern also showed the crater effect, where the signal intensity will decrease over time because the plasma is continuously more confined in the developing crater.

The raster pattern provided (relatively) constant laser energy but used up too much area since the pattern had to be spread out to cover pristine sample surface with every new line. As the standards were scarce, this pattern was not the optimal solution either.

Line scans presented the best option for these types of experiments and were a compromise between analyzing sufficient area and providing efficient and feasible measurement patterns. A typical ablation pattern consisted of at least 200 warmup shots and 50 shots per line. Through the use of warmup shots and even warmup lines the strongly deviating laser energy, whose typical progression for a pattern with five lines is depicted in Figure 15, could be somewhat compensated. To reach a plateau of constant energy, at least 200 warmup shots, which were fired into the shutter, were needed. As

Figure 15 shows, the laser energy starts at a value of 3,5 mJ and increases to ca. 6 mJ during the warmup shots after the third line. However, in the time it takes the device to close the shutter, the energy decreases to 5 mJ again. For the actual shots the energy rises approximately from 5 mJ to 6 mJ with a relative standard deviation (RSD) of up to 20 % which is expected for LIBS experiments. Due to the laser generating reproducible energies starting with usually the third line, the first two lines featuring lower energies and therefore less intense signals were discarded as warmup lines. This had to be considered when designing the experiment and two extra lines were added in every ablation pattern. The laser energy was determined by the internal power meter of the J200, which was placed at the end of the beam path before the laser irradiated the sample. As it was not properly calibrated, a value of 6 mJ (100 %) would amount to approximately 7 mJ on the sample surface.

Warmup shots were always fired with 100 % laser energy and the velocity for the line scan was 0,5 mm/s for most experiments.

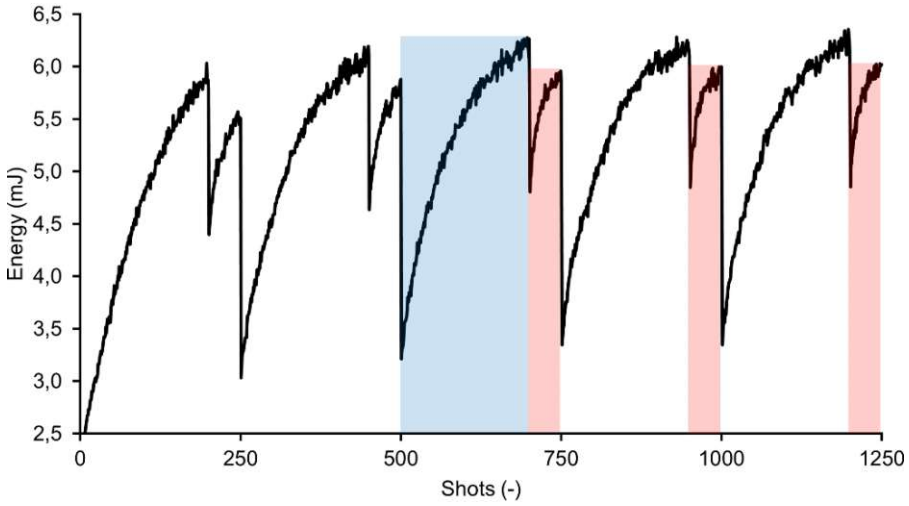

Figure 15: Typical laser energy curve of the J200 LIBS instrument during measurement of an ablation pattern consisting of 5 consecutive lines with 200 warmup shots (highlighted in blue for the third line) and 50 shots (red) per line, totaling 1250 shots. The laser energy was very inconsistent with a relative standard deviation (RSD) of up to 20 % within the same line and an overall increase. This energy was determined by the internal power meter of the J200, which was placed at the end of the beam path before the laser irradiated the sample.

The results of the deviating laser energy can be seen in Figure 16, where the first two lines of the pattern led to less ablation than the following three due to lower laser energy. As a consequence, the resulting spectra also showed less intensity due to the strong dependence on the laser energy as explained in sections 2.1 and 2.6.

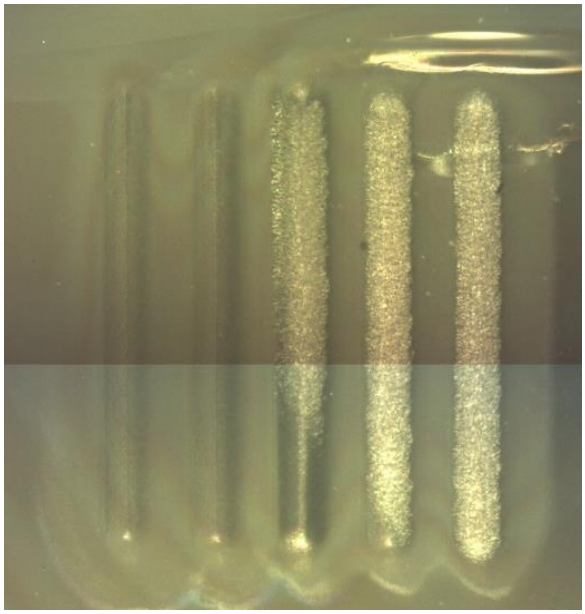

Figure 16: Ablation craters on the surface of a polymer matrix resulting from five consecutive line scans. The craters exhibited different depths due to the high variation in laser energy. Since the laser energy steadily increased throughout the pattern (from left to right), the last line expectedly led to the strongest ablation.

4.1.2 DS sample height

Before direct sampling could be employed, the sample height in the custom-made DS had to be optimized, as the exact position of the fiber entrance relative to the plasma plume had a major impact on the signal intensity (cf. section 2.4.2). To achieve this, the entire floor of the ablation chamber was covered with Al foil and heat maps (the emission intensity is recorded as a function of the x and y coordinates) at different sample heights were measured. The investigated sample heights were 0 mm, 1 mm, 1,5 mm, 2 mm, 2,5 mm, and 3 mm, though only four sample heights are shown in Figure 17. Al foil was chosen as a favorable specimen because of two reasons. Firstly, it could be easily cut to a fitting circular shape encompassing the chamber floor. Secondly, the Al I 396,1 nm emission line[14] exhibited very high intensity and could therefore be detected sufficiently using less harsh laser settings providing for a feasible measurement, especially considering the prolonged duration of a heat map covering 6 × 6 mm^2 sample area. The custom 3D printed spacers mentioned in section 3.1.4 also proved to be very practical for this task.

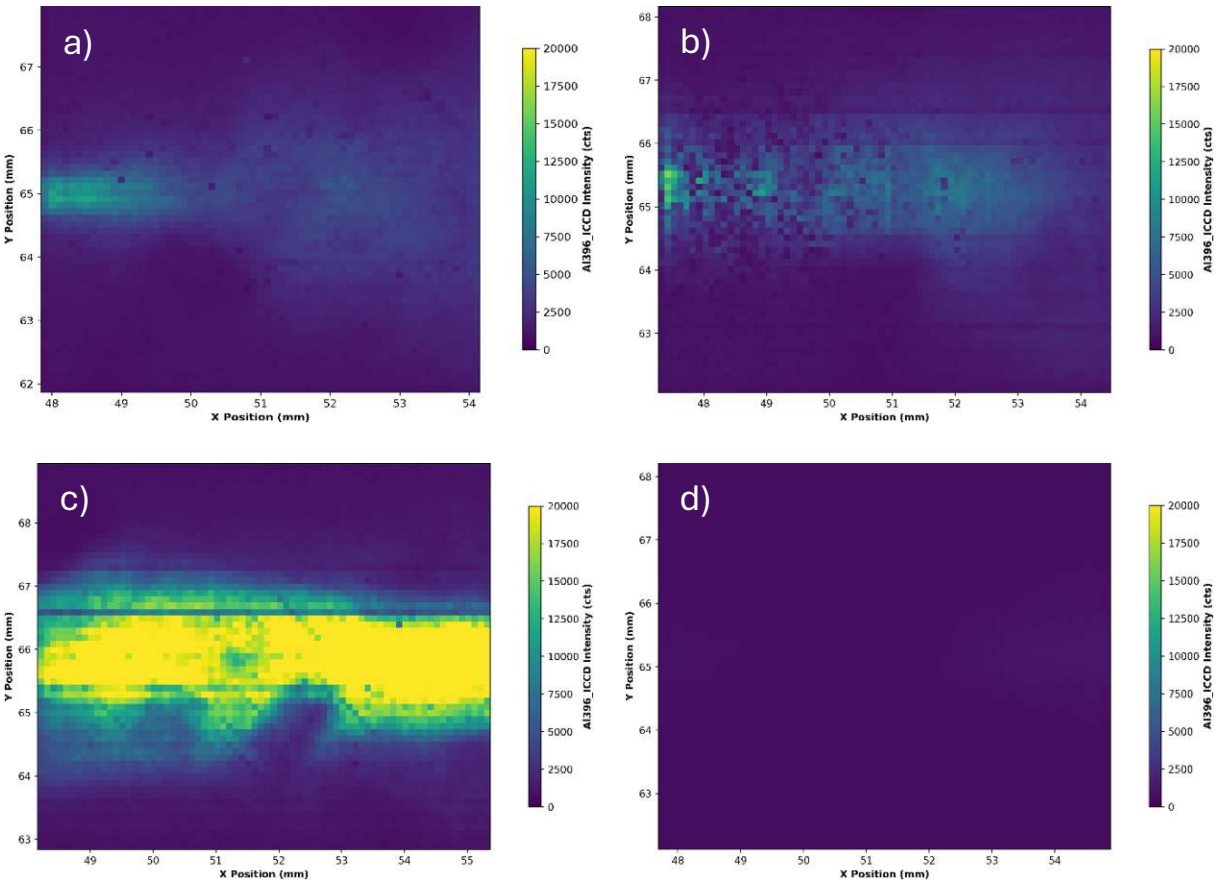

Figure 17: Sample height optimization of the direct stage (DS) using Al foil and the intensity of the Al I 396,1 nm emission line at different sample heights of a) 0 mm, b) 1 mm, c) 2 mm, and d) 3 mm in the ablation chamber. The optimal sample height was determined to be 2 mm though the restricted field of view of the fiber optic cable resulted in an 'intense corridor' across the middle of the chamber with little to no intensity at the top and bottom.

The results of the sample height optimization for the DS are shown in Figure 17. As could be expected, they confirmed the strong dependence of the signal intensity on the sample and subsequently the plasma plume position. A sample height of 2 mm led to the best signals, as Figure 17c depicts, and was therefore chosen as the optimal sample height in the DS ablation chamber. The restricted field of view of the fiber optic cable, however, resulted in the occurrence of an 'intense corridor' approximately 1,5 mm wide across the middle of the chamber, which was in axis with the entrance of the fiber on the right side of the ablation chamber, with little to no intensity at the top and bottom. A sample height of 1 mm (see Figure 17b) displayed the same restrictions where only the area farthest to left had sufficient height to become visible. These experiments emphasized the importance of being mindful of the sample position at any given time as a LIBS operator, as it can have detrimental effects on the outcome of experiments.

4.2 Fluorine

4.2.1 Optimization including pressure variation

To give an insight into the optimization process of an element with low intensity emissions, and to show what a LIBS spectrum generally looks like, the variation of the spectrometer gate delay for the 2172 µg/g F standard is shown in Figure 18. As the gate delay determines the time between the laser ablation and the recording of the spectrometer, it is one of the most important parameters in LIBS experiments. A change of the gate delay therefore has a major effect on the spectrum and whether emission lines of certain elements are visible at all.

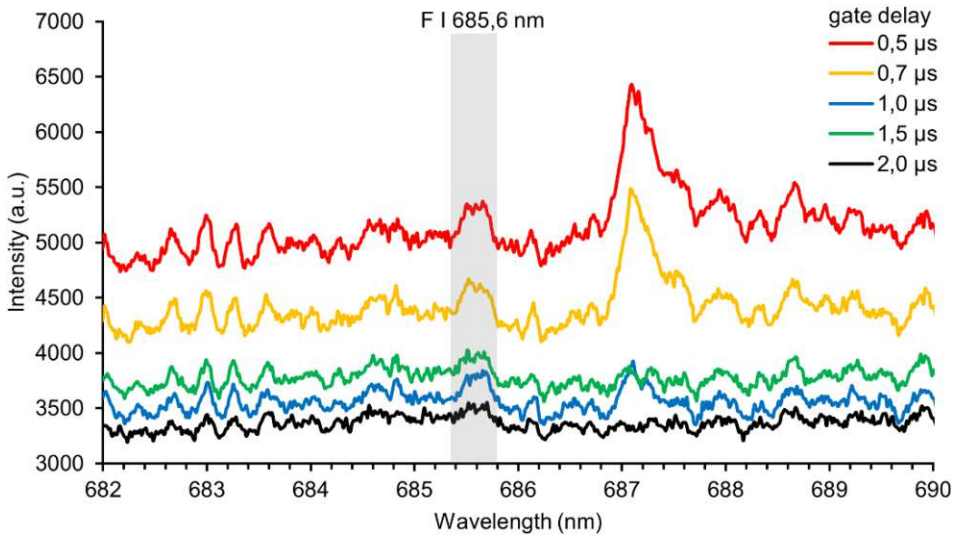

Figure 18: Gate delay optimization for F detection (2172 µg/g F in PI standard) in a 1 L/min Ar atmosphere at 1013 mbar, 61 raw LIBS spectra were averaged. The intensity of the F I 685,6 nm emission line increased with decreasing gate delay.

During the gate delay variation values from 0,5 µs to 2,0 µs were applied while all other parameters were held constant. As Figure 18 indicates, a shorter gate delay resulted in enhanced signal intensity for the F I emission line[14] at 685,6 nm (the 'I' denotes emission lines of a neutral F atom) and background. While the signal was not visible for 2,0 µs, F can at least be considered evident for 0,5 µs though there is of course further optimization needed to obtain an adequate peak. The overall intensity of the spectrum also increased from ~3500 a.u. to 5000 a.u. with decreasing gate delay, whereas the optimal gate delay for F was later determined to be 0,3 µs. This variation was carried out using the newly developed DS at 1013 mbar and an Ar flow of 1 L/min, while the spectrometer was set to a center wavelength of 686 nm with a gate width of 5 µs and 400 µm slit width. The laser shot an ablation pattern consisting of 1 line with 61 shots which were averaged at ~7 mJ laser energy and a spot size of 100 µm.

The most important step towards a quantitative LIBS method for F was the application of reduced pressure. As a result of changing plasma dynamics, as discussed in section 2.3, the quality of the signal could be enhanced drastically. To investigate the dependence of F emission line intensity on the pressure in the ablation chamber a pressure variation was carried out. The pressures tested ranged as low as 50 mbar, which was the lowest pressure the vacuum pump (cf. section 3.1.3) could achieve while purging with a He flow of 0,2 L/min. To be able to clearly assign the changes in the spectrum to the different pressures, all remaining parameters were again held constant.

Figure 19 depicts the results of the pressure optimization for the 2172 µg/g standard and indicates that the use of vacuum greatly improved the intensity of the F I 685,6 nm emission line. He atmosphere additionally led to less intense but narrower peaks compared to Ar, which was beneficial for the SNR. Besides the narrower peak shape, the use of He resulted in the absence of the interfering Ar I 687,2 nm emission line[14]. This serves as a reminder that the choice of atmosphere should always be considered in LIBS experiments.

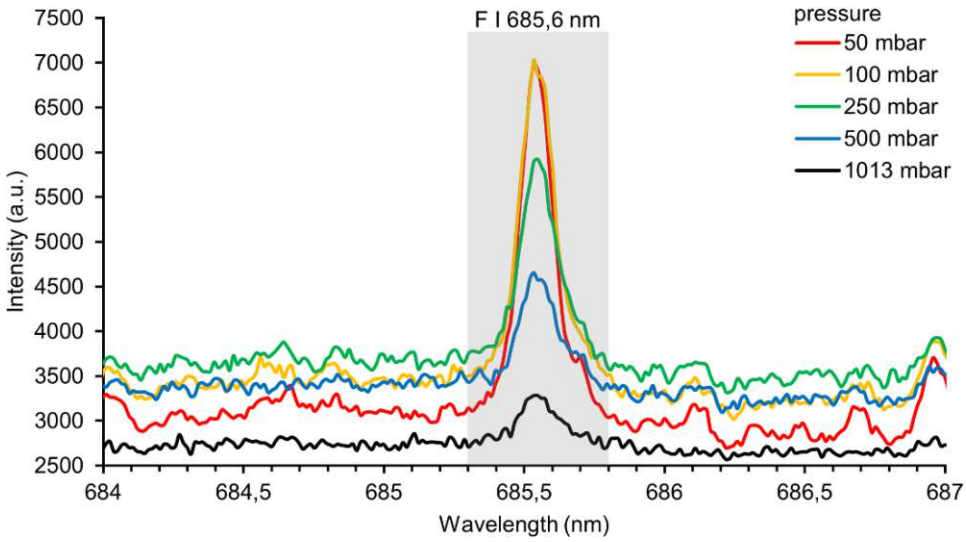

Figure 19: Pressure optimization for F detection (2172 µg/g F in PI standard) in a 0,2 L/min He atmosphere with 0,3 µs gate delay, 61 raw LIBS spectra were averaged. The intensity of the F I 685,6 nm emission line increased with decreasing pressure, resulting in an improvement of the SBR by a factor of ~2.

The signal-to-background ratios of the pressure optimization in Figure 19 are listed in Table 4 and proved that the use of vacuum is favorable for the detection of F in LIBS experiments. Through the application of 50 mbar, which was determined to be the optimal pressure, the SBR could be improved by a factor of ~2 compared to measurements under atmospheric pressure. To summarize, the combination of vacuum and He atmosphere led to higher signal intensity and narrower peak shape resulting in a better SBR.

Table 4: Signal-to-background ratios (SBR) for the F I 685,6 nm emission line (2172 µg/g F in PI standard) at reduced pressures according to the measurements in Figure 19 in a 0,2 L/min He atmosphere. Through the application of reduced pressure, the SBR could be improved by a factor of ~2.

Pressure (mbar)	SBR (-)
1013	1,2
500	1,4
250	1,6
100	2,0
50	2,2

As a proof of concept, the material of a sports bag containing a fluoropolymer coating was analyzed using this method. The significant enhancement in signal quality is shown in Figure 20.

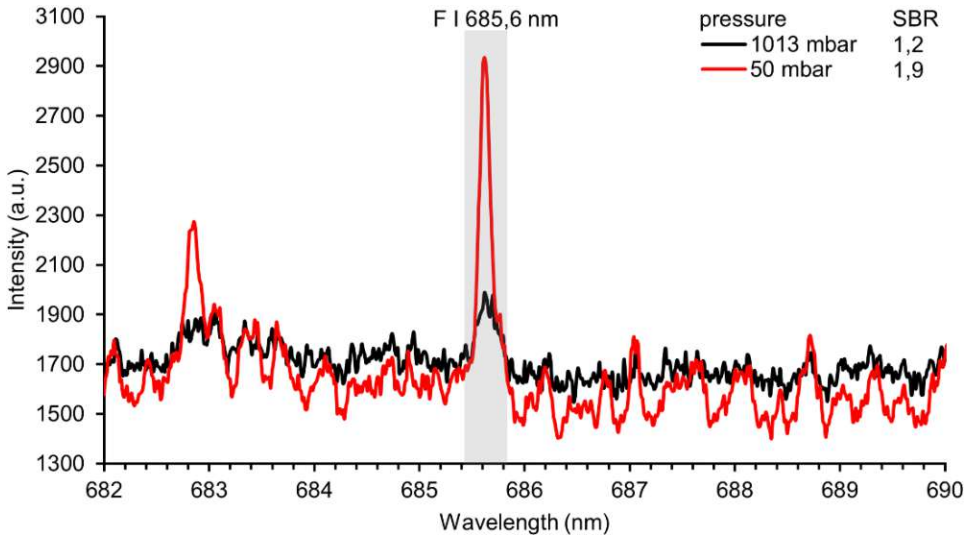

Figure 20: Material of a sports bag containing a fluoropolymer coating analyzed using the 50 mbar LIBS method. The enhancement in signal quality in comparison to atmospheric pressure can be recognized by the increased SBR.

As the pressure optimization was conducted using the HS and sampling via collection optics, the potential of direct sampling, meaning collection of the plasma emissions directly next to the plume with a fiber optic cable as explained in section 2.4.2, was investigated next. After the optimization of the DS sample height a reasonable comparison between the HS and the DS could be made. To be able to compare the two stages properly, measurements of the 2172 µg/g F standard were carried out with the exact same parameters. To highlight the benefit of reduced pressure these were conducted with and without vacuum. The He flow was set to 0,2 L/min for all experiments and 61 spectra were averaged to obtain the following results in Figure 21. Immediately, the higher absolute intensity of the DS compared to the HS could be noticed. This now

thoroughly optimized method provided orders of magnitude better signals for the same standard than it did at the start of the process in Figure 18 for instance.

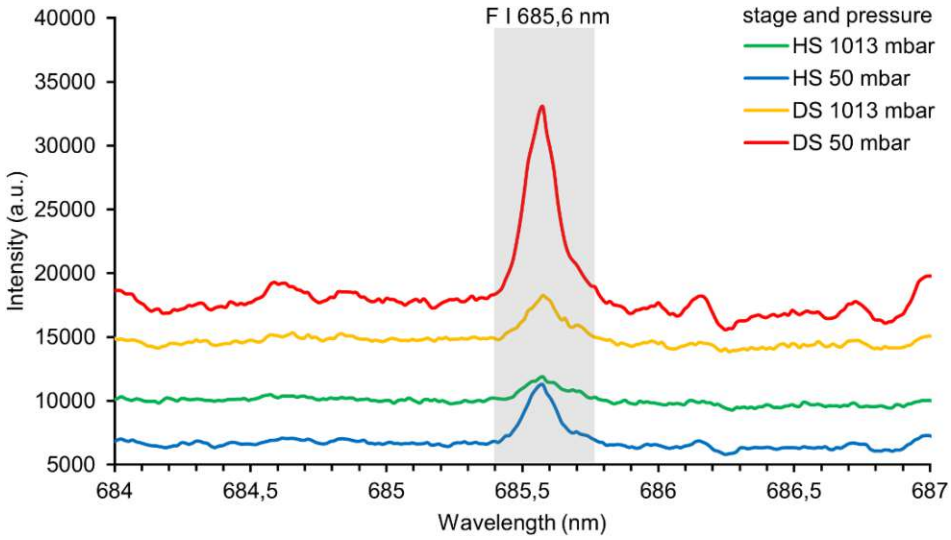

Figure 21: Comparison of the heating stage (HS, sampling with collection optics) and direct stage (DS, sampling with fiber optic cable) with and without vacuum for the F I 685,6 nm emission line (2172 µg/g F in PI standard) detection. The He flow was set to 0,2 L/min for all experiments, the remaining parameters were held constant as well. A general increase in signal intensity could be noted for the DS.

To maintain a quantitative approach the SBRs of the peaks in Figure 21 were calculated. They are listed in Table 5 and confirmed the visual impression that the DS led to better signals. This applies equally to the measurements under atmospheric pressure and at 50 mbar, where the SBR of the DS reached a value of 1,8 compared to 1,1 for the HS without vacuum. The highest SBR could be achieved using vacuum and direct sampling.

Table 5: Signal-to-background ratios (SBR) and peak heights (PH) of the heating stage (HS, sampling with collection optics) and direct stage (DS, sampling with fiber optic cable) with and without vacuum for the F I 685,6 nm emission line (2172 µg/g F in PI standard) in Figure 21. The He flow was set to 0,2 L/min for all experiments, the remaining parameters were held constant as well. The highest SBR could be achieved using vacuum and direct sampling, whereas the DS generally accomplished higher SBR than the HS.

Pressure (mbar)	SBR of HS (-)	SBR of DS (-)	PH of HS (a.u.)	PH of DS (a.u.)
1013	1,1	1,2	1489	3450
50	1,7	1,8	4553	15107

After the optimization of the method was finished, a calibration of the prepared standards could be measured. All optimized measurement parameters for the quantitative and fast determination of F in a polyimide coating are listed in the following Table 6. This includes laser settings, atmosphere and placement of the sample in the ablation chamber, light collection system, and spectrometer configuration.

Table 6: Optimized measurement parameters for F detection in polyimide coatings using LIBS under reduced pressure.

Laser: J200 LIBS instrument	
Laser energy	~7 mJ
Warmup shot energy	~7 mJ
Frequency	20 Hz
Spotsize	100 µm
Stage velocity	0,5 mm/s
Ablation pattern	
Lines	5
Warmup shots	400
Shots	61
Distance between parallel lines	300 µm
Ablation chamber	
Stage	DS
Sample height	2 mm
Gas flow	0,2 L/min He
Pressure	50 mbar
Spectrometer: SpectraPro HRS-750 with PI MAX 4	
Grating	1800 g/mm
Center wavelength	686 nm
Emission line	F I 685,6 nm
Gate delay	0,3 µs
Gate width	5 µs
Intensifier gain	50
Slit width	400 µm
1 line (61 spectra) averaged, first 2 lines discarded	

4.2.2 Calibration

The quantitative analysis consisted of performing a calibration utilizing the F standards prepared in section 3.2 and the optimized measurement parameters for the DS given in Table 6 at the end of the corresponding section 4.2.1. The standards composed of F in PI ranged from 27 to 2172 µg/g F including a blank. The collected data was then normalized employing various normalization approaches detailed in section 2.6 and subsequently analyzed using linear regression. To be able to properly evaluate the quality of the calibrations, the analytical figures of merit coefficient of determination (R^2), root mean square error (RMSE), and limit of detection (LOD) were calculated according to section 2.7. The LOD was obtained from the calibration curve using all standards. To emphasize the beneficial effect of reduced pressure, the calibration was carried out at atmospheric pressure as well as 50 mbar, which was the optimal pressure determined for F as explained in section 4.2.1. The results of the F calibration in the form of R^2, RMSE, and LOD for various normalizations and at atmospheric pressure as well as 50 mbar are shown in Table 7.

Table 7: Results of the F calibration at atmospheric pressure and 50 mbar. The standards consisting of F in PI ranged from 27 to 2172 µg/g F including a blank (see Table 3) and the measurement parameters are listed in Table 6. The coefficient of determination (R^2), root mean square error (RMSE), and limit of detection (LOD) are listed for different types of normalizations. Normalization to the background and total area achieved the best analytical figures of merit confirming that normalization is essential in LIBS experiments. The measurements at 50 mbar always resulted in superior figures of merit proving that reduced pressure is beneficial for the determination of F in polymer coatings using LIBS.

Normalization method	Pressure (mbar)	R^2 (-)	RMSE (µg/g)	LOD (µg/g)
Background (BG)	1013	0,9253	201	767
	50	0,9988	25	95
Internal standard (IS), intensity	1013	0,9386	181	690
	50	0,9902	71	269
Internal standard (IS), area	1013	0,9636	138	524
	50	0,9757	112	426
Total area (TA)	1013	0,9378	182	695
	50	0,9977	34	131
Subtraction (SUB)	1013	0,9916	65	248
	50	0,9731	118	449
Unnormalized, intensity	1013	0,2867	1117	4256
	50	0,7445	415	1581
Unnormalized, area	1013	0,8037	350	1333
	50	0,9373	183	698

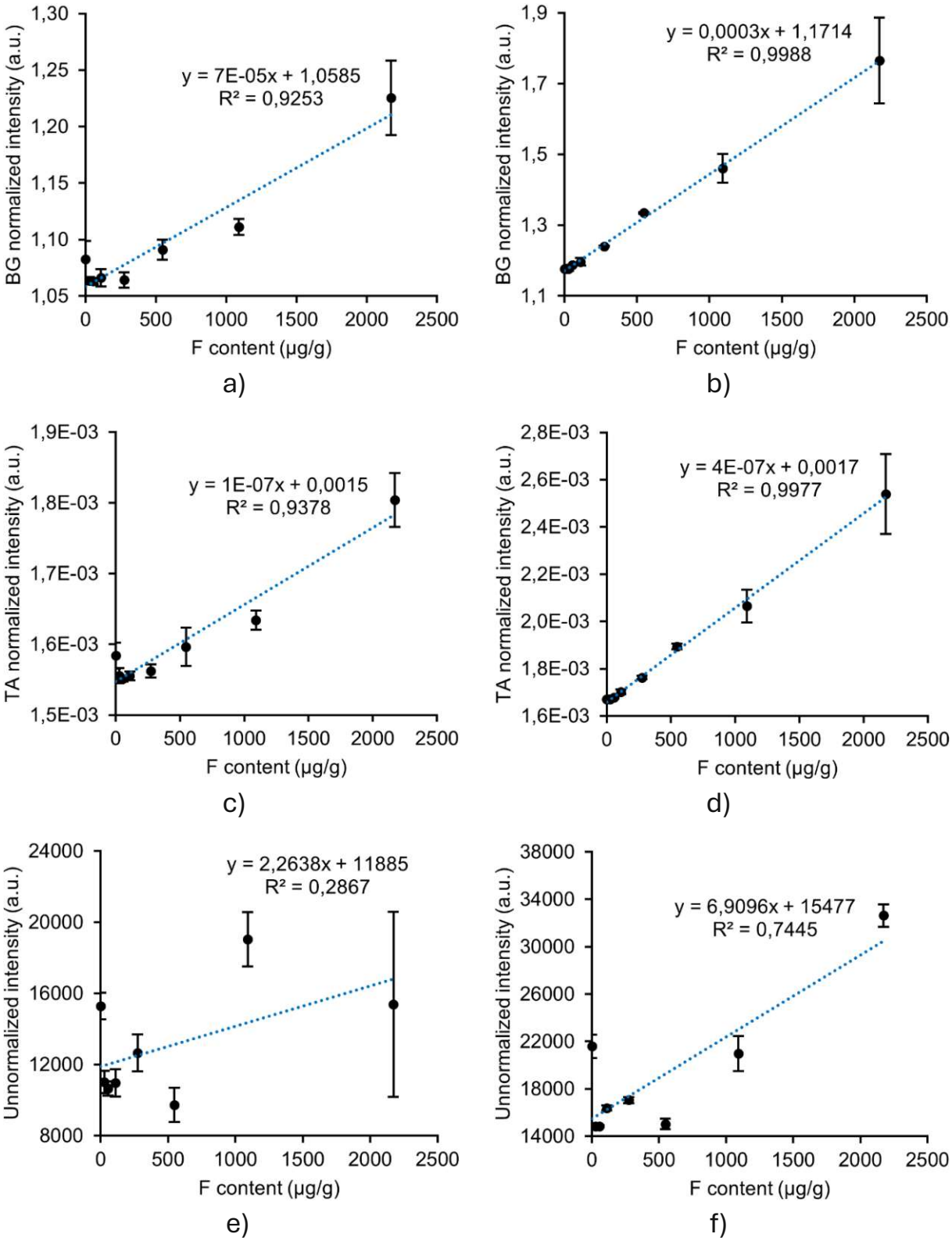

Figure 22: Comparison of differently normalized F calibration curves at atmospheric pressure and 50 mbar: a) BG and 1013 mbar, b) BG and 50 mbar, c) TA and 1013 mbar, d) TA and 50 mbar, e) unnormalized and 1013 mbar, f) unnormalized and 50 mbar. The background (BG) and total area (TA) normalized data led to calibration curves with much higher quality compared to the unnormalized data. The use of vacuum always resulted in better analytical figures of merit (cf. Table 7).

In Figure 22 the calibration curves that achieved the best analytical figures of merit, namely those obtained by normalization to the background and total area, are compared to the calibration curves obtained from unnormalized peak intensities of the F I 685,6 nm emission line.

The unnormalized data expectedly led to the worst results with the calibration using the intensity at 1013 mbar (Figure 22e) having a R^2 of 0,2867 and a LOD of 4256 µg/g, which is higher than the highest standard concentration. It was also prone to huge signal fluctuations typical for low quality LIBS experiments[35,53]. This is not surprising, as normalization is essential in LIBS[35], although the unnormalized area calibration at 50 mbar at least reached a R^2 of 0,9373. The use of vacuum drastically improved both calibrations.

Normalization to an internal standard, where an unspecified constant peak at 688,6 nm was used, revealed better calibrations than anticipated (normally internal standards need to fulfill strict requirements[35]) with all calibration curves possessing R^2 values higher than 0,93. The IS intensity calibration at 50 mbar even managed to achieve a R^2 of 0,9902 with a RMSE of 71 µg/g. Nonetheless, the LOD were too high for this method to be considered successful. The same can be said for normalization via subtraction, which was interestingly the only case where the measurement under reduced pressure resulted in worse analytical figures of merit. This effect could not be explained in this thesis.

The best results were achieved utilizing normalization to the background and total area, which is why they are well-established in LIBS[35]. Especially the measurements at 50 mbar provided calibrations of high quality with R^2 values greater than 0,99. The BG normalized calibration (Figure 22b) had a R^2 of 0,9988 along with a RMSE of only 25 µg/g and a LOD of 95 µg/g, which was the lowest LOD of all measurements. The TA normalized one (Figure 22d) almost faired equally as good obtaining a R^2 of 0,9977 with RMSE = 34 µg/g and LOD = 131 µg/g.

According to literature[45,54], the LOD should be calculated using standards ‘in the same concentration range’. Although there is no standardized procedure as to how wide this range should be, a LOD obtained from the five lowest standards (0-274 µg/g) would certainly represent a more accurate value. However, this method of calculation was not applicable to all calibrations because some calibration curves had a negative slope (for the five lowest data points). This is why the LOD in Table 7 was determined using all standards, maintaining a consistent approach. Nonetheless, the more accurate value for the LOD of the background normalized F calibration was 48 µg/g as well as 49 µg/g for the total area normalized F calibration. This was a remarkable result considering the low excitation efficiency shown by F and represented a lower limit of detection than some recent publications (160 µg/g by Weiss et al.[20], 135 µg/g by Quarles et al.[55], 65 µg/g by Pořízka et al.[56]). To summarize, the application of reduced pressure improved the quantification of F using LIBS.

4.3 Chlorine

As the use of reduced pressure significantly improved the quality of F measurements, the same was expected for Cl, which is a halogen with similar chemical properties. The Cl method also needed to be optimized first, though this will not be covered in such detail as in the previous section 4.2.1.

4.3.1 Optimization including pressure variation

To investigate the effect of reduced pressure on Cl signal intensity, pressure variation experiments were conducted as in Figure 19, ranging from 1013 to 50 mbar. These preliminary experiments revealed the optimal pressure for Cl detection to be 50 mbar, although 100 mbar almost had the same impact. In order to re-examine the potential of the DS, a comparison was carried out between the DS and the HS at atmospheric pressure and in vacuum. The results of these comparisons are presented in Figure 23 below.

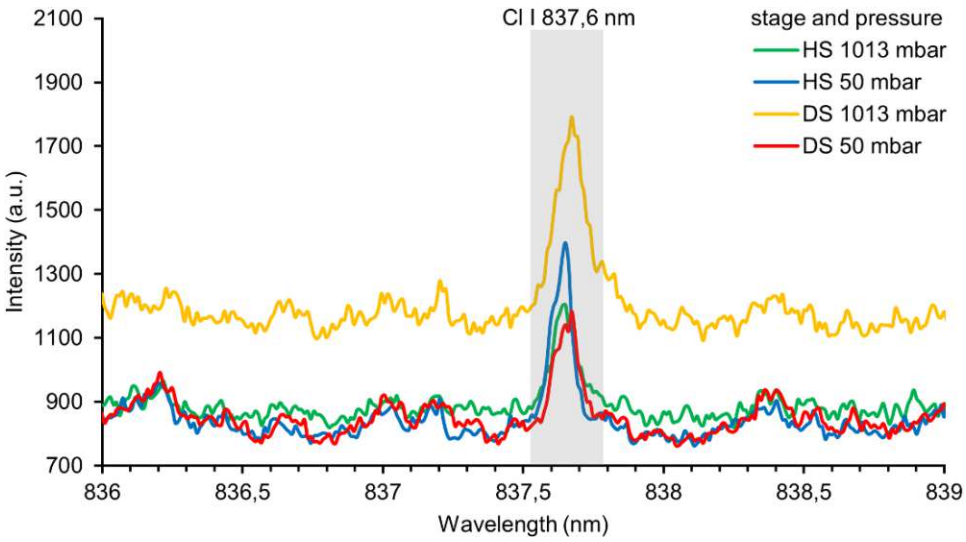

Figure 23: Comparison of the heating stage (HS, sampling with collection optics) and direct stage (DS, sampling with fiber optic cable) with and without vacuum for the Cl I 837,6 nm emission line (2552 µg/g Cl in PI standard) detection. While the He flow was set to 1 L/min for experiments at 1013 mbar, the measurements at 50 mbar had to be carried out using a He flow of 0,2 L/min. The remaining parameters were held constant. Although the DS at 1013 mbar resulted in elevated signal intensity, this effect was notably absent in a vacuum. The use of vacuum resulted in slightly enhanced signals when the HS was employed.

As Figure 23 shows, the use of vacuum slightly enhanced the signals when the HS was employed, which was excepted. Although the DS at 1013 mbar also resulted in elevated signal intensity, as it was the case in Figure 21, this effect was notably absent in vacuum where the intensity and quality of the signal rather resembled the HS. The cause for this unexpected outcome remained unknown, even after extensive tests with various sample

heights. However, it was assumed that the placement of the fiber optic cable was not compatible with the geometry of the plasma plume in the vacuum.

The signal-to-background ratios of the peaks in Figure 23 may be derived from Table 8. They confirmed that the application of 50 mbar led to a slight enhancement in signal quality for the HS with the SBR increasing from 1,4 to 1,7. With a SBR of 1,5 at 1013 mbar the DS achieved a higher value than the HS at the same pressure, thereby once again demonstrating its potential.

Table 8: Signal-to-background ratios (SBR) of the heating stage (HS, sampling with collection optics) and direct stage (DS, sampling with fiber optic cable) with and without vacuum for the Cl I 837,6 nm emission line (2552 µg/g F in PI standard) in Figure 23. While the He flow was set to 1 L/min for experiments at 1013 mbar, the measurements at 50 mbar had to be carried out using a He flow of 0,2 L/min. The remaining parameters were held constant. Although the DS at 1013 mbar resulted in a higher SBR than the HS at the same pressure, this beneficial impact was notably absent in vacuum.

Pressure (mbar)	SBR of HS (-)	SBR of DS (-)
1013	1,4	1,5
50	1,7	1,4

All optimized measurement parameters for the quantitative and fast determination of Cl in a polyimide coating are listed in the following Table 9. This includes laser settings, atmosphere in the ablation chamber, light collection system, and spectrometer configuration.

Table 9: Optimized measurement parameters for Cl detection in polyimide coatings using LIBS under atmospheric and reduced pressure.

Laser: J200 LIBS instrument	
Laser energy	~7 mJ
Warmup shot energy	~7 mJ
Frequency	20 Hz
Spotsize	100 µm
Stage velocity	0,5 mm/s
Ablation pattern	
Lines	5
Warmup shots	200
Shots	50
Distance between parallel lines	300 µm
Ablation chamber	
Stage	HS
Gas flow	0,2 or 1 L/min He
Pressure	50 or 1013 mbar
Spectrometer: SpectraPro HRS-750 with PI MAX 4	
Grating	1800 g/mm
Center wavelength	839 nm
Emission line	Cl I 837,6 nm
Gate delay	0,5 µs
Gate width	0,5 µs
Intensifier gain	50
Slit width	200 µm
1 line (50 spectra) averaged, first 2 lines discarded	

4.3.2 Calibration

The quantitative analysis utilized the Cl standards prepared in section 3.2 and the optimized measurement parameters given in Table 9 at the end of the corresponding section 4.3.1. As the DS was not available at the time, the HS was used for the calibration. Given that the discrepancy in signal quality between 1013 mbar and 50 mbar was not immense, the calibration was performed under both atmospheric conditions. The standards compromised of Cl in PI ranged from 1014 to 9500 µg/g Cl including a blank. Different normalization methods were tested, but only BG and TA yielded satisfactory results for the analysis of the Cl data. The analytical figures of merit were calculated in accordance with section 2.7, whereby all data points in the calibration curve were used to determine the LOD. The results of the Cl calibration in the form of R^2, RMSE, and LOD for two different normalizations can be derived from Table 10, along with the calibration curves in Figure 24.

Table 10: Results of the Cl calibration at atmospheric pressure and 50 mbar. The standards consisting of Cl in PI ranged from 1014 to 9500 µg/g Cl including a blank (see Table 3) and the measurement parameters are listed in Table 9. The coefficient of determination (R^2), root mean square error (RMSE), and limit of detection (LOD) are listed for two different types of normalizations. Normalization to the background and normalization to the total area yielded very similar analytical figures of merit. Surprisingly, the calibrations without vacuum achieved better results.

Normalization method	Pressure (mbar)	R^2 (-)	RMSE (µg/g)	LOD (µg/g)
Background (BG)	1013	0,9925	321	1497
	50	0,9745	597	2786
Total area (TA)	1013	0,9905	362	1688
	50	0,9798	530	2472

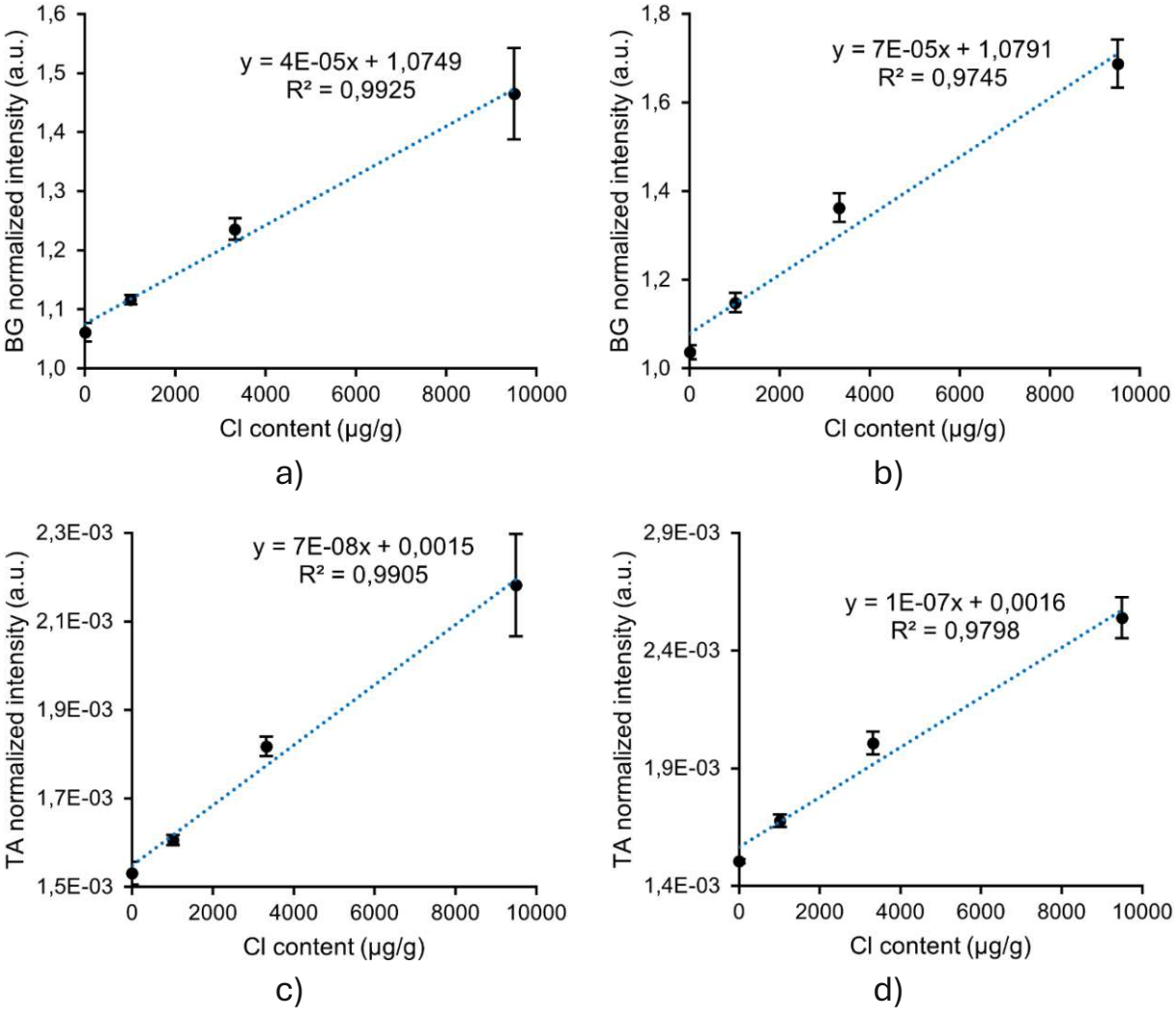

Figure 24: Comparison of differently normalized Cl calibration curves at atmospheric pressure and 50 mbar: a) BG and 1013 mbar, b) BG and 50 mbar, c) TA and 1013 mbar, d) TA and 50 mbar. Normalization to the background and normalization to the total area yielded very similar analytical figures of merit. Surprisingly, the calibrations without vacuum achieved better results (cf. Table 10).

Although the HS measurements at 50 mbar exhibited improved SBR in Table 8 and higher sensitivity in Figure 24 ($6{,}6 \cdot 10^{-5}$ a.u./(µg/g) at 50 mbar vs. $4{,}2 \cdot 10^{-5}$ a.u./(µg/g) at 1013 mbar), the calibration under atmospheric pressure achieved better figures of merit for both normalization methods. The BG normalized calibration at 1013 mbar led to the best results with an R^2 of 0,9925, a RMSE of 321 µg/g, and a LOD of 1497 µg/g. For the TA normalized calibration without vacuum, similar values were obtained. Apart from a passable R^2, the vacuum calibrations showed significantly worse RMSE and LOD. In conclusion, the Cl method proved to be less effective than the F method. Furthermore, the enhanced sensitivity resulting from the application of vacuum could not be employed in a quantitative manner, for reasons that remain unknown. One assumption is that the placement of the fiber optic cable was not compatible with the geometry of the plasma plume in the vacuum.

4.4 Bromine

Given the efficacy of vacuum LIBS in determining F and, at least qualitatively, in the measurement of Cl, it was reasonable to assume that it would also yield certain improvements in the determination of Br, the third halogen investigated in this thesis.

4.4.1 Optimization including pressure variation

To follow the approach employed in this work, a pressure variation using the HS was carried out (DS was not available) to investigate the effect that reduced pressure had on the Br sample spectrum. The pressures tested ranged as low as 50 mbar, while all remaining parameters, apart from the He flow, which was set to 1 L/min for 1013 mbar instead of 0,2 L/min, were held constant as usual. Figure 25 depicts the results of the pressure variation for the 11117 µg/g standard and indicates that the use of vacuum deteriorated the intensity of the Br I 827,3 nm emission line. Apparently, the changes in plasma dynamics stemming from the application of reduced pressure were detrimental to Br detection.

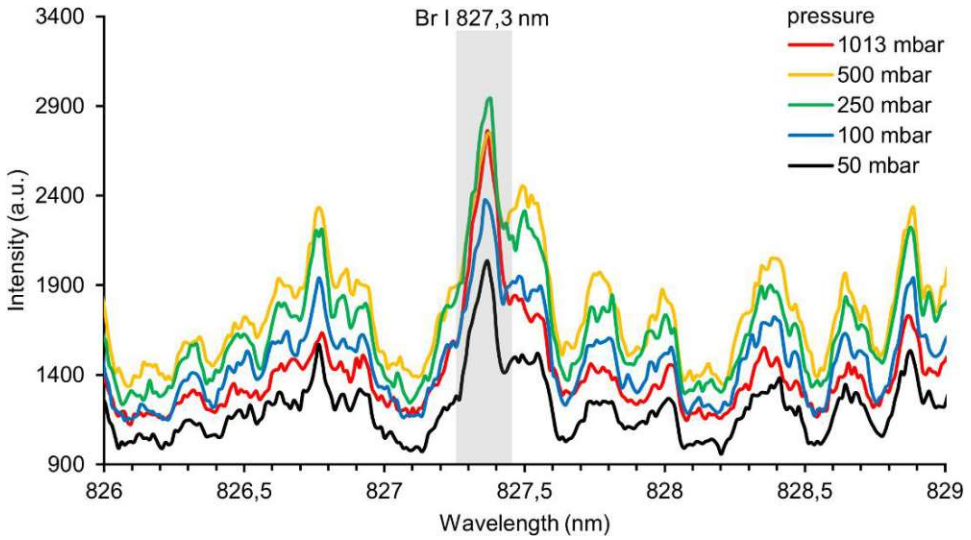

Figure 25: Pressure variation for Br detection (11117 µg/g Br in PI standard) with 0,5 µs gate delay, 41 raw LIBS spectra were averaged. While the He flow was set to 1 L/min for the experiment at 1013 mbar, the measurements at 50 mbar had to be carried out using a He flow of 0,2 L/min. The remaining parameters were held constant. The intensity of the Br I 827,3 nm emission line decreased with decreasing pressure, resulting in a decline in signal quality.

The actual Br signal, the area marked in grey in Figure 25, could be observed as the left shoulder of the peak, with the right shoulder being unspecified background. As this background increases with decreasing pressure (cf. 1013 mbar (red) and 100 mbar (blue) in the aforementioned illustration), the signal quality of Br I 827,3 nm also declines.

Subsequently, the Br method was optimized for operation at atmospheric pressure, which was conducted in the same manner as in sections 4.2.1 and 4.3.1. All optimized measurement parameters for the determination of Br in a polyimide coating are listed in the following Table 11. This includes laser settings, atmosphere in the ablation chamber, light collection system, and spectrometer configuration.

Table 11: Optimized measurement parameters for Br detection in polyimide coatings using LIBS at atmospheric pressure.

Laser: J200 LIBS instrument	
Laser energy	~7 mJ
Warmup shot energy	~7 mJ
Frequency	20 Hz
Spotsize	100 µm
Stage velocity	0,5 mm/s
Ablation pattern	
Lines	5
Warmup shots	200
Shots	50
Distance between parallel lines	300 µm
Ablation chamber	
Stage	HS
Gas flow	1 L/min He
Pressure	1013 mbar
Spectrometer: SpectraPro HRS-750 with PI MAX 4	
Grating	1800 g/mm
Center wavelength	828,4 nm
Emission line	Br I 827,3 nm
Gate delay	0,5 µs
Gate width	0,5 µs
Intensifier gain	50
Slit width	400 µm
1 line (50 spectra) averaged, first 2 lines discarded	

4.4.2 Calibration

The Br standards prepared in section 3.2 and the optimized measurement parameters given in Table 11 were used to perform the Br calibration with subsequent linear regression analysis. The standards compromised of Br in PI ranged from 119 to 11117 µg/g Br including a blank. Because the BG normalization had yielded the best results, it was employed for the analysis of the Br data. The analytical figures of merit were calculated in accordance with section 2.7, whereby all standards in the calibration curve except the highest one were used to determine the LOD. Because the concentration of the highest standard (11117 µg/g) was far apart from the remainder (all of them having contents lower than 35 % of the highest content), the highest standard was omitted from the evaluation. Its inclusion would have risked making the calibration unrobust, which means that the data point farthest away has more influence on the calibration curve. This could have resulted in a false impression regarding the calibration curve's quality, as the R^2 reached a value of 0,96 when the highest standard was included. The calibration curve along with the values for R^2, RMSE, and LOD of the background normalized data can be derived from Figure 26.

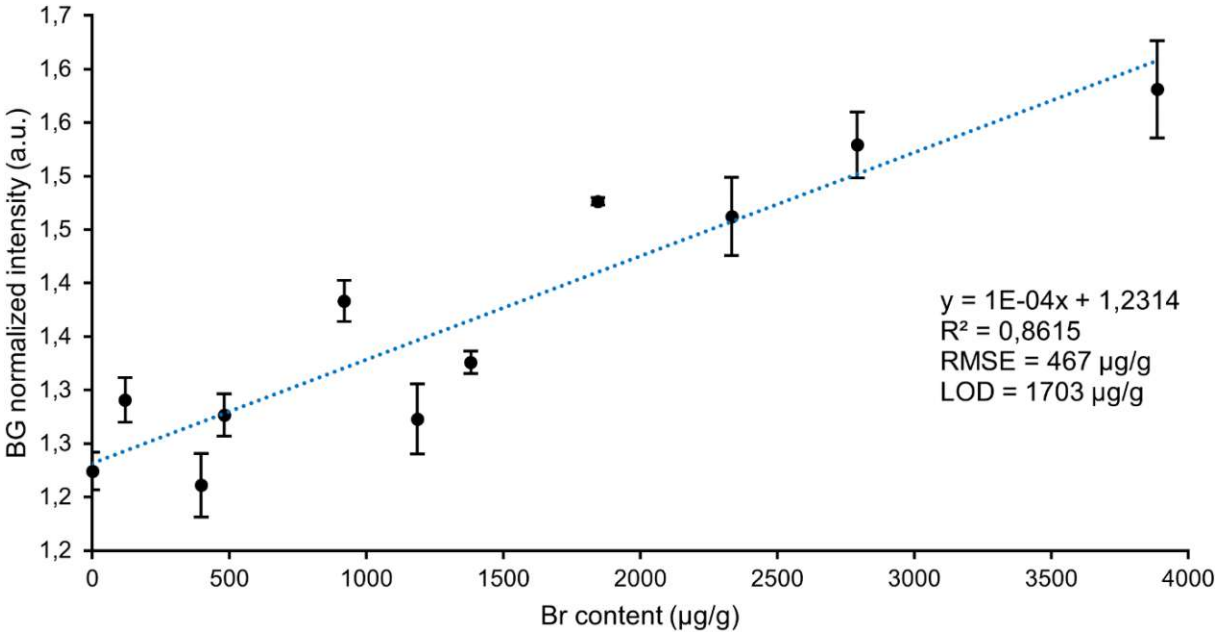

Figure 26: Result of the BG normalized Br calibration at atmospheric pressure with a He gas flow of 1 L/min. The standards consisting of Br in PI ranged from 119 to 3887 µg/g Br including a blank, see Table 3, and the measurement parameters are listed in Table 11. The coefficient of determination (R^2), root mean square error (RMSE), and limit of detection (LOD) are shown below the calibration function. Normalization to the background was used as it had provided the best results.

Considering the relatively low excitation efficiency of Br in LIBS, as for all halogens, the results of the calibration were as expected. The calibration curve exhibited a R^2 of 0,8615 along with a RMSE of 467 µg/g, which is the highest expected error of all calibrations in this thesis. Upon examination of the LOD, it becomes evident that with a value of 1703 µg/g it also was the most deficient of all. To summarize, while this method allows for the determination of Br, its analytical figures of merit are inferior to those of the F or Cl methods and further improvements are necessary to ensure its suitability for the analysis of real samples.

5 Conclusion & Outlook

The goal of this thesis was to develop a LIBS method that would allow the quantitative analysis of F, Cl, and Br in polymer coatings with limits of detection in the low µg/g range. In order to obtain signals of sufficient quality, the emission line intensities of the halogens, exhibiting relatively low excitation efficiencies, needed to be enhanced. One method of enhancement in LIBS is the application of reduced pressure to intensify the signals, though this is dependent on plasma dynamics and does not guarantee success for every element. Another option is the collection of the plasma radiation in the near vicinity of the plasma plume using a fiber optic cable instead of collection optics placed further away. This approach, referred to as 'direct sampling' in this work, may also lead to significantly higher signal intensities resulting from better collection efficiency, although the proper alignment of the fiber with respect to the plasma plume is crucial. These two different approaches could be investigated through the successful development of the 'direct stage', a custom-built ablation chamber mounted on a 3D printed stage built in-house.

To quantitatively analyze halogens, method optimizations and subsequent calibrations were performed utilizing this direct stage and prepared standards. These standards were also fabricated using in-house materials and consisted of halogenated polymers, produced by dissolving polyimide in NMP and spiking it with solutions of various halogen contents. The solutions were then applied to Si wafers or Al foil and the solvent evaporated on a heating plate, thereby obtaining solid halogenated polymer coatings with known halogen contents.

The method optimization for F showed great promise, as the application of vacuum significantly improved the signal intensity. By reducing the pressure in the ablation chamber to 50 mbar, the signal-to-background ratio of the F I 685,6 nm emission line could be increased by a factor of ~2. Determination of the peak area instead of the height might result in further improvements. Because of the strong signal fluctuation experienced in LIBS, a normalization of the data is necessary. To identify the normalization with the best efficacy for these types of experiments, different methods were investigated, including background, total area, internal standard, subtraction, and unnormalized. The best results were achieved utilizing normalization to the background and total area, which is why they are well-established in LIBS. The measurements at 50 mbar provided calibrations of high quality with R^2 values greater than 0,99. The background normalized calibration had a R^2 of 0,9988 along with a RMSE of only 25 µg/g and a LOD of 48 µg/g, which was the lowest LOD accomplished in this thesis and even lower than some recent publications ranging from 65-160 µg/g. The total area normalized one almost faired equally as good obtaining a R^2 of 0,9977 with RMSE = 34 µg/g and LOD = 49 µg/g. The quantitative analysis of F can therefore be considered a success, as was the application of the developed vacuum method to a fluoropolymer sample from industry (sports bag material).

Although the Cl measurements at 50 mbar exhibited improved SBR and higher sensitivity, the calibration under atmospheric pressure achieved better figures of merit. The background normalized calibration at 1013 mbar led to the best results with an R^2 of 0,9925, a RMSE of 321 µg/g, and a LOD of 1497 µg/g. For the total area normalized calibration without vacuum, similar values were obtained. Apart from a passable R^2, the vacuum calibrations showed significantly worse RMSE and LOD. In conclusion, the Cl method proved to be less effective than the F method. Furthermore, the enhanced sensitivity resulting from the application of vacuum could not be employed in a quantitative manner, for reasons that remain unknown. One assumption is that the placement of the fiber optic cable was not compatible with the geometry of the plasma plume in the vacuum.

Unfortunately, the use of vacuum did not have a beneficial effect on the Br I 827,3 nm emission line intensity. Therefore, the Br calibration was carried out in atmospheric conditions. Considering the relatively low excitation efficiency of Br in LIBS, the results of the Br calibration were as expected. The calibration curve exhibited a R^2 of 0,8615 along with a RMSE of467 µg/g, which is the highest expected error of all calibrations in this thesis. Upon examination of the LOD, it becomes evident that with a value of 1703 µg/g it also was the most deficient of all. To summarize, the Br method was not suitable enough for a quantitative analysis and could therefore not be considered a success in this work.

Looking ahead, the further development of the so-called ‘direct stage’, which collects the plasma radiation with a fiber optic cable directly next to the sample, should definitely be considered. By implementing a moveable stage inside the ablation chamber, the difficulties of finding a suitable sample position in relation to the entrance of the fiber optic cable could be mitigated. This way, the application of reduced pressure and the optimization of the sample position could be performed simultaneously. Given that the placement of the fiber represented the biggest challenge regarding the quantitative analysis of Cl, it is plausible that the issue could be addressed through this proposed device. The ablation chamber itself should be enlarged, as this would allow for more samples to be placed inside the chamber resulting in a more efficient and flexible method. In addition, the already small amount of sample preparation required would be reduced to virtually zero, as the wafers would not even need to be cut to size.

Besides the application of reduced pressure, numerous methods exist for enhancing the intensity of emission lines in LIBS experiments. Among these, several are currently the subject of research, including: double-pulse (collinear mode, orthogonal mode, crossed-beam mode; use of a second laser as an additional excitation source), magnetic confinement (plasma expansion confined by magnetic field), spark discharge (high voltage in a fast pulse discharge circuit), glow discharge (additional excitation through glow discharge), microwave assisted (microwave radiation originating from antenna elongating plasma lifetime), resonance enhancement (wavelength of second pulse is tuned to a resonant atomic transition of the plasmas matrix atoms), nanoparticle

enhancement (deposition of metallic nanoparticles on sample surface before irradiation), increased sample temperature, and flame enhancement (plasma generated in a flame leading to increased intensity). While the implementation of these techniques can be expensive and challenging in terms of instrumentation, the spatial confinement method (laser-induced plasma confined by cavity placed on sample surface) represents a considerably more feasible option.[29,57–59]

Spatial confinement could provide a cost-effective method with relatively easy implementation, considering the required cavities can be constructed in-house by 3D printing. The next logical step would be to ascertain the applicability of this method for halogen detection, Cl and Br in particular.

Bibliography

(1) Osenbach, J. W. Corrosion-Induced Degradation of Microelectronic Devices. *Semicond. Sci. Technol.* **1996**, *11* (2), 155–162. https://doi.org/10.1088/0268-1242/11/2/002.

(2) Kiddee, P.; Naidu, R.; Wong, M. H. Electronic Waste Management Approaches: An Overview. *Waste Management* **2013**, *33* (5), 1237–1250. https://doi.org/10.1016/j.wasman.2013.01.006.

(3) Brunnbauer, L.; Zeller, V.; Gajarska, Z.; Larisegger, S.; Schwab, S.; Lohninger, H.; Limbeck, A. Classification of Epoxy Molding Compounds by Tandem LA-ICP-MS/LIBS to Enhance the Reliability of Electronic Devices. *Spectrochimica Acta Part B: Atomic Spectroscopy* **2023**, *207*, 106739. https://doi.org/10.1016/j.sab.2023.106739.

(4) Kusoglu, A.; Weber, A. Z. New Insights into Perfluorinated Sulfonic-Acid Ionomers. *Chem. Rev.* **2017**, *117* (3), 987–1104. https://doi.org/10.1021/acs.chemrev.6b00159.

(5) Adhikari, B.; Majumdar, S. Polymers in Sensor Applications. *Progress in Polymer Science* **2004**, *29* (7), 699–766. https://doi.org/10.1016/j.progpolymsci.2004.03.002.

(6) Milani, P.; França, D.; Balieiro, A. G.; Faez, R. Polymers and Its Applications in Agriculture. *Polímeros* **2017**, *27* (3), 256–266. https://doi.org/10.1590/0104-1428.09316.

(7) Maitz, M. F. Applications of Synthetic Polymers in Clinical Medicine. *Biosurface and Biotribology* **2015**, *1* (3), 161–176. https://doi.org/10.1016/j.bsbt.2015.08.002.

(8) Burkarter, E.; Saul, C. K.; Thomazi, F.; Cruz, N. C.; Roman, L. S.; Schreiner, W. H. Superhydrophobic Electrosprayed PTFE. *Surface and Coatings Technology* **2007**, *202* (1), 194–198. https://doi.org/10.1016/j.surfcoat.2007.05.012.

(9) Gowariker, V. R.; Viswanathan, N. V.; Sreedhar, J. *Polymer Science*; Wiley: New York, 1986.

(10) Dhanumalayan, E.; Joshi, G. M. Performance Properties and Applications of Polytetrafluoroethylene (PTFE)—a Review. *Adv Compos Hybrid Mater* **2018**, *1* (2), 247–268. https://doi.org/10.1007/s42114-018-0023-8.

(11) Goosey, M. Degradation and Hydrolysis of Polymers Used in Semiconductor Processing, Assembly and Packaging. *Polymer Degradation and Stability* **1987**, *17* (3), 237–252. https://doi.org/10.1016/0141-3910(87)90066-8.

(12) Luo, G.-B.; Pang, B.; Luo, X.-Q.; Wang, Y.; Zhou, H.; Zhao, L.-J. Brominated Butyl Rubber Anticorrosive Coating and Its Self-Healing Behaviors. *Chin J Polym Sci* **2023**, *41* (2), 297–305. https://doi.org/10.1007/s10118-022-2844-8.

(13) *Fluorine: Chemistry, Analysis, Function and Effects*; Preedy, V. R., Ed.; Royal Society of Chemistry: Cambridge, 2015.

(14) Kramida, A.; Ralchenko, Y. NIST Atomic Spectra Database, NIST Standard Reference Database 78, 1999. https://doi.org/10.18434/T4W30F.

(15) Edlén, B. On the Identification of Ar x and Ar Xiv in the Solar Corona and the Origin of the Unidentified Coronal Lines. *Sol Phys* **1969**, *9* (2), 439–445. https://doi.org/10.1007/BF02391668.

(16) Yang, L.; Gao, H.; Zhou, J.; Ng, C. Y. VACUUM ULTRAVIOLET LASER PHOTOION AND PULSED FIELD IONIZATION–PHOTOION STUDY OF RYDBERG SERIES OF CHLORINE ATOMS PREPARED IN THE ^2P_J (J = 3/2 and 1/2) FINE-STRUCTURE STATES. *ApJ* **2015**, *810* (2), 132. https://doi.org/10.1088/0004-637X/810/2/132.

(17) Huffman, R. E.; Larrabee, J. C.; Tanaka, Y. New Absorption Series and Ionization Potentials of Atomic Fluorine, Chlorine, Bromine, and Iodine. *The Journal of Chemical Physics* **1967**, *47* (2), 856–857. https://doi.org/10.1063/1.1711962.
(18) Schultes, L.; Peaslee, G. F.; Brockman, J. D.; Majumdar, A.; McGuinness, S. R.; Wilkinson, J. T.; Sandblom, O.; Ngwenyama, R. A.; Benskin, J. P. Total Fluorine Measurements in Food Packaging: How Do Current Methods Perform? *Environ. Sci. Technol. Lett.* **2019**, *6* (2), 73–78. https://doi.org/10.1021/acs.estlett.8b00700.
(19) Alvarez-Llamas, C.; Pisonero, J.; Bordel, N. A Novel Approach for Quantitative LIBS Fluorine Analysis Using CaF Emission in Calcium-Free Samples. *J. Anal. At. Spectrom.* **2017**, *32* (1), 162–166. https://doi.org/10.1039/C6JA00386A.
(20) Weiss, M.; Gajarska, Z.; Lohninger, H.; Marchetti-Deschmann, M.; Ramer, G.; Lendl, B.; Limbeck, A. Elemental Mapping of Fluorine by Means of Molecular Laser Induced Breakdown Spectroscopy. *Analytica Chimica Acta* **2022**, *1195*, 339422. https://doi.org/10.1016/j.aca.2021.339422.
(21) *Laser-Induced Breakdown Spectroscopy: Theory and Applications*; Musazzi, S., Perini, U., Eds.; Springer Series in Optical Sciences; Springer Berlin Heidelberg: Berlin, Heidelberg, 2014; Vol. 182. https://doi.org/10.1007/978-3-642-45085-3.
(22) Cremers, D. A.; Radziemski, L. J. *Handbook of Laser-Induced Breakdown Spectroscopy*, Second edition.; Wiley: Chichester, 2013.
(23) Brunnbauer, L. *Laser-Induced Breakdown Spectroscopy (LIBS)*. https://www.tuwien.at/tch/lalibs/techniken/libs (accessed 2024-07-20).
(24) Hussain Shah, S. K.; Iqbal, J.; Ahmad, P.; Khandaker, M. U.; Haq, S.; Naeem, M. Laser Induced Breakdown Spectroscopy Methods and Applications: A Comprehensive Review. *Radiation Physics and Chemistry* **2020**, *170*, 108666. https://doi.org/10.1016/j.radphyschem.2019.108666.
(25) Limbeck, A.; Brunnbauer, L.; Lohninger, H.; Pořízka, P.; Modlitbová, P.; Kaiser, J.; Janovszky, P.; Kéri, A.; Galbács, G. Methodology and Applications of Elemental Mapping by Laser Induced Breakdown Spectroscopy. *Analytica Chimica Acta* **2021**, *1147*, 72–98. https://doi.org/10.1016/j.aca.2020.12.054.
(26) Xu, F.; Ma, S.; Zhao, C.; Dong, D. Application of Molecular Emissions in Laser-Induced Breakdown Spectroscopy: A Review. *Front. Phys.* **2022**, *10*, 821528. https://doi.org/10.3389/fphy.2022.821528.
(27) Svelto, O. *Principles of Lasers*; Springer US: Boston, MA, 2010. https://doi.org/10.1007/978-1-4419-1302-9.
(28) *What are Nd:YAG Lasers? - GoPhotonics.com*. https://www.gophotonics.com/community/what-are-nd-yag-lasers (accessed 2024-07-28).
(29) Li, Y.; Tian, D.; Ding, Y.; Yang, G.; Liu, K.; Wang, C.; Han, X. A Review of Laser-Induced Breakdown Spectroscopy Signal Enhancement. *Applied Spectroscopy Reviews* **2018**, *53* (1), 1–35. https://doi.org/10.1080/05704928.2017.1352509.
(30) Effenberger, A.; Scott, J. Effect of Atmospheric Conditions on LIBS Spectra. *Sensors* **2010**, *10* (5), 4907–4925. https://doi.org/10.3390/s100504907.
(31) Yalçın, Ş.; Tsui, Y. Y.; Fedosejevs, R. Pressure Dependence of Emission Intensity in Femtosecond Laser-Induced Breakdown Spectroscopy. *J. Anal. At. Spectrom.* **2004**, *19* (10), 1295–1301. https://doi.org/10.1039/B404132A.
(32) Fernández-Manteca, M. G.; Martínez-Minchero, M.; García-Escárzaga, A.; Ocampo-Sosa, A. A.; Mirapeix, J.; Valdiande, J. J.; López-Higuera, J. M.; Rodríguez-Cobo, L.; Cobo, A. Comparison of Light Capturing Approaches in Laser-Induced Breakdown

Spectroscopy (LIBS) for Multichannel Spectrometers. *Spectrochimica Acta Part B: Atomic Spectroscopy* **2023**, *201*, 106617. https://doi.org/10.1016/j.sab.2023.106617.

(33) Shabanov, S. V.; Gornushkin, I. B.; Winefordner, J. B. Radiation from Asymmetric Laser-Induced Plasmas Collected by a Lens or Optical Fiber. *Appl. Opt.* **2008**, *47* (11), 1745. https://doi.org/10.1364/AO.47.001745.

(34) Rao, A. P. Rapid Analysis of Plutonium Surrogate Material via Hand-Held Laser-Induced Breakdown Spectroscopy. Master Thesis, Air Force Institute of Technology, Wright-Patterson Air Force Base, 2020. https://rgdoi.net/10.13140/RG.2.2.18732.74888 (accessed 2024-08-02).

(35) Guezenoc, J.; Gallet-Budynek, A.; Bousquet, B. Critical Review and Advices on Spectral-Based Normalization Methods for LIBS Quantitative Analysis. *Spectrochimica Acta Part B: Atomic Spectroscopy* **2019**, *160*, 105688. https://doi.org/10.1016/j.sab.2019.105688.

(36) Lyčka, M.; Peska, V.; Demko, M.; Spyroglou, I.; Kilar, A.; Fajkus, J.; Fojtová, M. WALTER: An Easy Way to Online Evaluate Telomere Lengths from Terminal Restriction Fragment Analysis. *BMC Bioinformatics* **2021**, *22* (1), 145. https://doi.org/10.1186/s12859-021-04064-0.

(37) De Giacomo, A.; Dell'Aglio, M.; De Pascale, O.; Gaudiuso, R.; Santagata, A.; Teghil, R. Laser Induced Breakdown Spectroscopy Methodology for the Analysis of Copper-Based-Alloys Used in Ancient Artworks. *Spectrochimica Acta Part B: Atomic Spectroscopy* **2008**, *63* (5), 585–590. https://doi.org/10.1016/j.sab.2008.03.006.

(38) Dell'Aglio, M.; Gaudiuso, R.; Senesi, G. S.; De Giacomo, A.; Zaccone, C.; Miano, T. M.; De Pascale, O. Monitoring of Cr, Cu, Pb, V and Zn in Polluted Soils by Laser Induced Breakdown Spectroscopy (LIBS). *J. Environ. Monit.* **2011**, *13* (5), 1422. https://doi.org/10.1039/c0em00780c.

(39) Zorov, N. B.; Gorbatenko, A. A.; Labutin, T. A.; Popov, A. M. A Review of Normalization Techniques in Analytical Atomic Spectrometry with Laser Sampling: From Single to Multivariate Correction. *Spectrochimica Acta Part B: Atomic Spectroscopy* **2010**, *65* (8), 642–657. https://doi.org/10.1016/j.sab.2010.04.009.

(40) Senesi, G. S.; Dell'Aglio, M.; Gaudiuso, R.; De Giacomo, A.; Zaccone, C.; De Pascale, O.; Miano, T. M.; Capitelli, M. Heavy Metal Concentrations in Soils as Determined by Laser-Induced Breakdown Spectroscopy (LIBS), with Special Emphasis on Chromium. *Environmental Research* **2009**, *109* (4), 413–420. https://doi.org/10.1016/j.envres.2009.02.005.

(41) Hahn, D. W.; Omenetto, N. Laser-Induced Breakdown Spectroscopy (LIBS), Part II: Review of Instrumental and Methodological Approaches to Material Analysis and Applications to Different Fields. *Appl Spectrosc* **2012**, *66* (4), 347–419. https://doi.org/10.1366/11-06574.

(42) Barnett, W. B.; Fassel, V. A.; Kniseley, R. N. Theoretical Principles of Internal Standardization in Analytical Emission Spectroscopy. *Spectrochimica Acta Part B: Atomic Spectroscopy* **1968**, *23* (10), 643–664. https://doi.org/10.1016/0584-8547(68)80045-X.

(43) Body, D.; Chadwick, B. L. Optimization of the Spectral Data Processing in a LIBS Simultaneous Elemental Analysis System. *Spectrochimica Acta Part B: Atomic Spectroscopy* **2001**, *56* (6), 725–736. https://doi.org/10.1016/S0584-8547(01)00186-0.

(44) Fabre, C.; Cousin, A.; Wiens, R. C.; Ollila, A.; Gasnault, O.; Maurice, S.; Sautter, V.; Forni, O.; Lasue, J.; Tokar, R.; Vaniman, D.; Melikechi, N. In Situ Calibration Using Univariate Analyses Based on the Onboard ChemCam Targets: First Prediction of Martian Rock and Soil Compositions. *Spectrochimica Acta Part B: Atomic Spectroscopy* **2014**, *99*, 34–51. https://doi.org/10.1016/j.sab.2014.03.014.

(45) Shrivastava, A.; Gupta, V. Methods for the Determination of Limit of Detection and Limit of Quantitation of the Analytical Methods. *Chron Young Sci* **2011**, *2* (1), 21. https://doi.org/10.4103/2229-5186.79345.

(46) El Haddad, J.; Canioni, L.; Bousquet, B. Good Practices in LIBS Analysis: Review and Advices. *Spectrochimica Acta Part B: Atomic Spectroscopy* **2014**, *101*, 171–182. https://doi.org/10.1016/j.sab.2014.08.039.

(47) *J200 Laser-Induced Breakdown Spectroscopy (LIBS) Instrument*. Applied Spectra. https://appliedspectra.com/products/j200-libs-instrument.html (accessed 2024-07-14).

(48) *SpectraPro HRS-750 | Press Release*. Teledyne Princeton Instruments. https://www.princetoninstruments.com/news/new-spectrapro-hrs-750 (accessed 2024-07-14).

(49) *PI MAX 4*. Teledyne Princeton Instruments. https://www.princetoninstruments.com/products/pi-max-family/pi-max (accessed 2024-07-14).

(50) Gibbs, D. K. Using LA-ICP-MS for the Determination of Deuterium in an Effort to Analyze Water Absorption by Thin Polymer Films. Master Thesis, Technische Universität Wien, Wien, 2022.

(51) *Welch-Ilmvac 2115 Variable Speed Evaporator Auto Sensing Vacuum System – Chemtech Scientific Incorporated*. https://www.chemtechsci.com/products/welch-ilmvac-2115-variable-speed-evaporator-auto-sensing-vacuum-system (accessed 2024-07-18).

(52) Applied Spectra, Inc. Axiom 2.0 Software Manual For J200 Systems, 2020. https://support.appliedspectra.com/download/j-200-axiom-la-2-0-software-manual-rev1-1-1 (accessed 2024-02-07).

(53) Davari, S. A.; Taylor, P. A.; Standley, R. W.; Mukherjee, D. Detection of Interstitial Oxygen Contents in Czochralski Grown Silicon Crystals Using Internal Calibration in Laser-Induced Breakdown Spectroscopy (LIBS). *Talanta* **2019**, *193*, 192–198. https://doi.org/10.1016/j.talanta.2018.09.078.

(54) Mermet, J.-M. Limit of Quantitation in Atomic Spectrometry: An Unambiguous Concept? *Spectrochimica Acta Part B: Atomic Spectroscopy* **2008**, *63* (2), 166–182. https://doi.org/10.1016/j.sab.2007.11.029.

(55) Quarles, C. D.; Gonzalez, J. J.; East, L. J.; Yoo, J. H.; Morey, M.; Russo, R. E. Fluorine Analysis Using Laser Induced Breakdown Spectroscopy (LIBS). *J. Anal. At. Spectrom.* **2014**, *29* (7), 1238. https://doi.org/10.1039/c4ja00061g.

(56) Pořízka, P.; Kaski, S.; Hrdlička, A.; Modlitbová, P.; Sládková, L.; Häkkänen, H.; Prochazka, D.; Novotný, J.; Gadas, P.; Čelko, L.; Novotný, K.; Kaiser, J. Detection of Fluorine Using Laser-Induced Breakdown Spectroscopy and Raman Spectroscopy. *J. Anal. At. Spectrom.* **2017**, *32* (10), 1966–1974. https://doi.org/10.1039/C7JA00200A.

(57) Wang, Z.; Hou, Z.; Lui, S.; Jiang, D.; Liu, J.; Li, Z. Utilization of Moderate Cylindrical Confinement for Precision Improvement of Laser-Induced Breakdown Spectroscopy Signal. *Opt. Express* **2012**, *20* (S6), A1011. https://doi.org/10.1364/OE.20.0A1011.

(58) Guo, J.; Wang, T.; Shao, J.; Chen, A.; Jin, M. Emission Enhancement of Laser-Induced Breakdown Spectroscopy by Increasing Sample Temperature Combined with Spatial Confinement. *J. Anal. At. Spectrom.* **2018**, *33* (12), 2116–2123. https://doi.org/10.1039/C8JA00246K.

(59) Su, X.; Zhou, W.; Qian, H. Optimization of Cavity Size for Spatial Confined Laser-Induced Breakdown Spectroscopy. *Opt. Express* **2014**, *22* (23), 28437. https://doi.org/10.1364/OE.22.028437.

List of Figures

List of Tables